FINAL REPORT

Development and Evaluation of an Interactive Sub-Grid Cloud Framework for the CAMx Photochemical Model

AQRP Project 14-025
QA Requirements: Audits of Data Quality: 10% Required

Prepared for:
Gary McGaughey
Texas Air Quality Research Program
The University of Texas at Austin

Prepared by:
Christopher Emery, Jeremiah Johnson,
DJ Rasmussen, Wei Chun Hsieh, Greg Yarwood
Ramboll Environ
773 San Marin Drive, Suite 2115
Novato, California, 94998

John Nielsen-Gammon, Kenneth Bowman,
Renyi Zhang, Yun Lin, Leong Siu
Texas A&M University
Department of Atmospheric Sciences
College Station, Texas 77843

July 2015

06-25699J

ACKNOWLEDGMENT

The preparation of this report is based on work supported by the State of Texas through the Air Quality Research Program administered by The University of Texas at Austin by means of a Grant from the Texas Commission on Environmental Quality.

CONTENTS

TABLES

FIGURES

EXECUTIVE SUMMARY

Under Texas Air Quality Research Program (AQRP) Project 14-025, Ramboll Environ and collaborators at Texas A&M University (TAMU) incorporated an explicit sub-grid cloud model into the Comprehensive Air quality Model with extensions (CAMx) and evaluated its effects against aircraft measurements logged during two field study campaigns. This report documents the approach, implementation, and testing of the cloud model system. We are providing the new model to the Texas Commission on Environmental Quality (TCEQ); this update will be combined with other modifications and publicly released in a future version of CAMx.

The US Environmental Protection Agency (EPA) requires the use of photochemical grid models to demonstrate how local emission control plans will achieve the federal air quality standard for ground-level ozone in nonattainment areas designated as moderate or higher (EPA, 2014). There are currently two ozone nonattainment areas in the State of Texas but this number will likely increase with the promulgation of a stricter ozone standard in late 2015. TCEQ uses CAMx for both regulatory and research applications.

Daily convective cloudiness and rainfall are common occurrences throughout much of Texas and the southern US during the ozone season (typically April through October). Such convection most often occurs at small scales, and its ubiquity and abundance provide important mechanisms for exchanging boundary layer air with the free troposphere, for chemical processing, and for wet removal. Up to this point CAMx has not explicitly treated cloud processes at scales smaller than the grid resolution (1-10 km). While diagnosed sub-grid cloud fields have been used to parametrically influence grid-scale photolysis rates, wet deposition, and aqueous chemistry, CAMx has not included cloud convective transport.

The new “Cloud-in-Grid” (CiG) treatment includes a new vertical convective transport component for both in-cloud and ambient fractions of the grid column, as well as explicit aqueous chemistry and wet scavenging within the sub-grid cloud compartment. The CAMx/CiG is linked to updates to the Weather Research and Forecasting (WRF) meteorological model’s Kain-Fritsch (K-F) sub-grid cumulus scheme that has been recently improved by EPA’s National Exposure Research Laboratory (NERL). The new algorithm has been thoroughly quality assured, and process testing in serial and parallel modes indicates no substantial impact to overall model speed. The CiG offers two advantages over approaches employed in other off-line photochemical grid models: (1) a direct and consistent link between WRF and CAMx models that removes the need to independently re-diagnose convection location, depth, intensity, and water contents; and (2) the inclusion of both in-cloud convective fluxes and compensating vertical motions in the ambient portion of the cell.

CAMx/CiG was evaluated by applying the model to multi-day episodes in 2008 and 2013 when ozone and precursor concentration measurements were available from aircraft measurement campaigns during the 2008 Stratosphere-Troposphere Analyses of Regional Transport (START08) and the 2013 Deriving Information on Surface conditions from Column and Vertically Resolved Observations Relevant to Air Quality (DISCOVER-AQ), respectively. Specific days

during each episode were selected for the presence of various convective modes. The consequences of convective mixing on the horizontal and vertical distribution of key gas-phase constituents (ozone, nitrogen oxides and carbon monoxide) were qualitatively assessed for plausibility and were compared to aircraft observations in nearby locations and similar times.

We confirm that the convective mixing parameterization produces substantial changes in constituent mixing ratio in areas of model-simulated convection, with smaller yet potentially widespread contributions from regional convection. The CiG generally improves boundary layer simulations of ozone and nitrogen oxides when compared to aircraft-derived profiles. A relative lack of impact at aircraft-sampled locations in the 2008 episode is a consequence of insufficient model-simulated convection rather than any deficiency in the convective mixing parameterization. Based on the project results summarized in this report, we recommend follow-on projects that address additional evaluation and necessary extensions to other areas of the model.

1.0 INTRODUCTION

Under Texas Air Quality Research Program (AQRP) Project 14-025, Ramboll Environ and collaborators at Texas A&M University (TAMU) incorporated an explicit sub-grid cloud model into the Comprehensive Air quality Model with extensions (CAMx) and evaluated its effects against aircraft measurements logged during two field study campaigns. This report documents the approach, implementation, and testing of the cloud model system.

The US Environmental Protection Agency (EPA) requires the use of photochemical grid models to demonstrate how local emission control plans will achieve the federal air quality standard for ground-level ozone in nonattainment areas designated as moderate or higher (EPA, 2014). There are currently two ozone nonattainment areas in the State of Texas but this number will likely increase with the promulgation of a stricter ozone standard in late 2015. The Texas Commission on Environmental Quality (TCEQ) uses CAMx (ENVIRON, 2014) for both regulatory and research applications.

Daily convective cloudiness and rainfall are common occurrences throughout much of Texas and the southern US during the ozone season. Such convection most often occurs at small scales, and its ubiquity and abundance provide important mechanisms for exchanging boundary layer air with the free troposphere, for chemical processing, and for wet removal. Up to this point CAMx has not explicitly treated cloud processes at scales smaller than the grid resolution (1-10 km). While diagnosed sub-grid cloud fields have been used to parametrically influence grid-scale photolysis rates, wet deposition, and aqueous chemistry, CAMx has not included cloud convective transport.

1.1 Background

A large fraction of the cloud size spectrum is not explicitly resolved by the grid scales typically employed in regional meteorological and photochemical models. The physical effects from these “sub-grid” clouds are difficult to characterize accurately, but they can substantially influence many different atmospheric processes, including: boundary layer mixing, ventilation, and deep vertical transport of heat, moisture, and chemical tracers; radiative transfer and surface energy budgets; spatio-temporal precipitation patterns, intensity and wet scavenging rates; chemistry via photolysis and aqueous reactions; and certain environmentally-sensitive emission sectors (e.g., biogenics). Recently, Pan et al. (2014) observed transport of stratospheric ozone into the troposphere via deep convection, and note that proper representation of this process is a problem for coarse-resolution global models. An example of the types of finer-scale clouds regularly occurring across Texas and the US during the ozone season is shown in Figure 1.

Sub-grid cloud parameterizations are employed in meteorological models to adjust grid-resolved vertical profiles of heat and moisture from the effects of moist convection. The Kain-Fritsch (KF) convective parameterization (Kain, 2004) is perhaps the most widely used option in the Weather Research and Forecasting (WRF) model (Skamarock et al., 2008) when it is run to

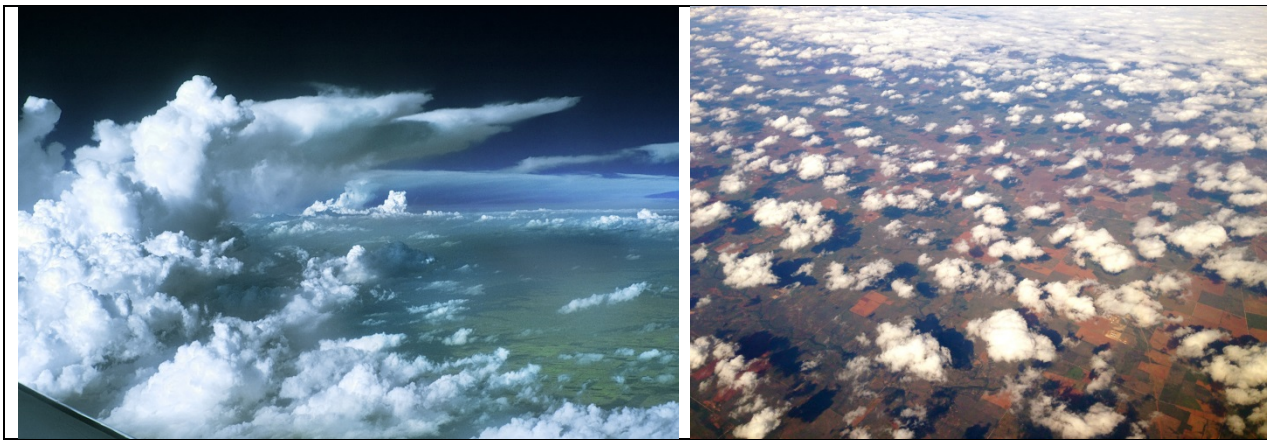

Figure 1. (Left) Example of scattered shallow and deep convection over Texas. (Right) A typical summer afternoon with scattered shallow cumulus over Texas

support "off-line" photochemical models like CAMx. However, such parameterizations in WRF have not historically interacted with other important processes such as radiative transfer, which can lead to errors in surface temperature and boundary layer mixing, and in turn feed back into the evolution of cloud and precipitation fields.

Researchers at EPA's National Exposure Research Laboratory (NERL) have made improvements to WRF by combining KF sub-grid cloud information with grid-scale cloud fields as input to WRF's radiation treatment (Alapaty et al., 2012: Herwehe et al., 2014a). They show that simulated surface temperature and precipitation fields with the new KF-radiation interaction ("RadKF") are improved relative to the unmodified version of WRF. More recently, the group has developed a new multi-scale treatment for KF ("MSKF"), which includes radiation feedback, to extend its applicability over a wider range of grid resolutions down to 1 km (Alapaty et al., 2013; 2014; Herwehe et al., 2014b).

From the air quality perspective, moist convection is an important component for long-range transport of ozone, particulate matter (PM), and precursors. The effects of sub-grid clouds on vertical transport, chemistry, and wet scavenging are addressed to varying degrees in "off-line"[1] photochemical models (Zhao et al., 2009; Foley et al., 2010; Belikov et al., 2013). Often, however, the spatial/temporal distributions of such clouds must be diagnosed indirectly because meteorological models do not export necessary information from their sub-grid cloud parameterizations. This leads to potentially large inconsistencies between the meteorological and air quality models.

Prior to this project, CAMx implicitly addressed the influence of sub-grid clouds by diagnosing their presence according to resolved wind and thermodynamic fields from meteorological

[1] In this context, the term "off-line" refers to air quality models that are run separately from the meteorological model that supplies environmental fields of winds, temperature, moisture, etc. "Coupled" models simulate the evolution of meteorology and air quality in lock-step within a single platform.

model output, and blending their properties into the resolved cloud fields (Emery et al., 2010). The final blended cloud fields were used to adjust photolysis rates, perform aqueous chemistry, and remove pollutants via wet scavenging at grid scale – no separate sub-grid cloud processes were explicitly treated. Furthermore, CAMx did not include a cloud convective mixing treatment.

Two recent studies by Kemball-Cook et al. (2012, 2013) have evaluated CAMx-simulated tropospheric nitrogen oxide (NOx) profiles throughout the south-central and eastern US against aircraft measurements and satellite remote sensing products. The comparison between CAMx and satellite nitrogen dioxide (NO_2) columns show that, like other regional and global models, CAMx underestimates NOx and its oxidation products (collectively referred to as NOy) at altitudes above 8 km (Kemball-Cook et al., 2012). Satellite instruments have higher sensitivity in the upper troposphere, so satellite-model column comparisons are more heavily weighted aloft and model errors aloft can confound the inter-comparisons. Particularly from this perspective, properly simulating NOy in the upper troposphere is crucial. Kemball-Cook et al. (2013) have conducted experiments that add high-altitude sources of NOx (aircraft and lightning), and extend boundary layer mixing deep into the upper troposphere in the presence of diagnosed sub-grid convection. Such enhancements improve, but do not altogether ameliorate, CAMx under predictions of NO_2 in the upper troposphere. More recently, Kemball-Cook et al. (2014a) have introduced explicit top boundary conditions for ozone and NOy from global models, and have increased vertical resolution in the upper troposphere, both of which further improve NOy performance aloft. The addition of sub-grid convection is yet another important increment for the proper treatment of NO_2 columns and NOy budgets aloft.

1.2 Objectives

The primary goal of this work is to introduce explicit sub-grid shallow and deep convective cloud mixing within CAMx. Further, we develop an approach to improve interactions with chemistry and wet deposition to operate explicitly at sub-grid scales in tandem with the cloud mixing scheme. Our work directly addresses two AQRP priority research areas: (1) improving the simulation of clouds in air quality modeling, especially at sub-grid-scales; and (2) global and regional transport of pollutants into Texas, using data collected by aircraft, ozonesondes, and satellites, and modeling analyses.

Our approach ties into NERL's recent WRF updates, whereby specific sub-grid cloud fields generated by RadKF and MSKF are passed to CAMx to define their spatial/temporal distributions and mixing rates for the sub-grid cloud algorithm in CAMx. This yields a consistent cloud-mixing-chemistry system across WRF and CAMx models.

The new CAMx treatment is tested for two convective episodes, one from the September 2013 Deriving Information on Surface conditions from Column and Vertically Resolved Observations Relevant to Air Quality (DISCOVER-AQ) field study in Houston (Pickering et al., 2013), and one from the Spring 2008 Stratosphere-Troposphere Analyses of Regional Transport (START08) field study over the south-central US (Pan et al., 2010). Tests particularly address convective impacts

to tropospheric profiles of NOy, ozone, and other chemical tracers by comparing to *in situ* concentration and tropospheric column profiles from aircraft measurements. We are providing the new model to TCEQ; this update will be combined with other modifications and publicly released in a future version of CAMx.

1.3 Report Organization

Section 2 describes the scientific theory, development, and preliminary testing of the CAMx sub-grid cloud modeling system. Section 3 presents analyses and results from model applications during the aircraft measurement campaigns. Section 4 summarized quality assurance steps conducted in this project. Section 5 summarizes results from this study and presents our recommendations.

2.0 DEVELOPMENT AND PRELIMINARY TESTING

2.1 Design

The KF cumulus parameterization is fundamentally a mass flux scheme. In WRF, changes to grid-scale temperature and moisture are calculated from the parameterized properties of entraining/detraining plumes that constitute convective updrafts and downdrafts, and from ambient compensating subsidence outside the cloud necessary to maintain mass conservation. This places the KF scheme within a subset of cumulus parameterization schemes for which constituent transport is already implicit.

Ramboll Environ has developed and implemented an interactive sub-grid cloud framework in CAMx v6.10 to address shallow mixing, deep convective transport, aqueous chemistry, and wet scavenging. All processes are driven by optional output fields generated by the WRF meteorological model's KF cumulus parameterization (Kain, 2004) as recently updated by NERL (Alapaty et al., 2012, 2013, 2014; Herwehe et al., 2014a,b). This yields a consistent cloud-mixing system across the WRF and CAMx models.

The CAMx sub-grid cloud framework operates separately from the normal grid processes in a manner similar to the Plume-in-Grid (PiG) model (Emery et al., 2013a; ENVIRON, 2014). This "cloud-in-grid" (CiG) approach defines the physical attributes of a multi-layer cloud volume according to newly available time-varying KF cloud data output by WRF. Each CiG configuration is unique to each grid column (or entirely absent from it) and characterizes a stationary, steady-state, sub-grid cloud environment between each meteorological update time. Fractions of grid-scale pollutant concentration profiles within each grid column are allocated to the CiG, which then operates on those fractional profiles to include convective transport, entrainment/ detrainment exchange with the ambient column, chemistry, and wet removal.

2.1.1 Coupling WRF to CAMx

Requisite meteorological fields are passed from WRF to CAMx via an interface program called WRFCAMx. This interface also diagnoses certain fields that are not directly available from WRF (e.g., vertical diffusion rates) based on well-established relationships among the available fields. The CAMx CiG framework is coupled exclusively to NERL's RadKF and MSKF treatments. WRFCAMx reads and processes two- and three-dimensional (2-D and 3-D) WRF fields that are specific to the KF algorithm, including:

- 3-D shallow and deep cloud fractions (CLDFRA_SH, CLDFRA_DP, unitless)
- 3-D sub-grid cloud water and ice mixing ratios (QC_CU, QI_CU, kg/kg)
- 3-D horizontal updraft and downdraft entrainment and detrainment flux profiles (UER, UDR, DER, DDR, kg/s)
- 2-D convective time scale (TIMEC, s)

These specific variables must be listed in the WRF output registry and flagged for output. Only cloud fractions and cloud water/ice profiles are listed in the output registries of released

versions of WRF. We have further modified WRF to pass the KF flux and time scale variables to the WRF output registry. These updates will be sent to the National Center for Atmospheric Research (NCAR) so that they may be included in a future version of WRF. Meanwhile, groups wishing to use this modeling system can obtain the modified WRF source code directly from Ramboll Environ.

If a WRF cumulus parameterization other than RadKF or MSKF is run, or the needed KF variables are not output, then WRFCAMx must be run with the original diagnostic cloud calculations, and CAMx reverts back to addressing only grid scale processes with its original parameterized influences from diagnosed sub-grid clouds.

In general, WRFCAMx passes the WRF variables listed above directly to the CAMx cloud/rain input file, with two exceptions. First, the 3-D shallow and deep cloud fractions are added and vertically averaged to yield a single 2-D cloud fraction field. Second, as with other meteorological variables, the entrainment/detrainment flux profiles and sub-grid cloud water/ice contents are vertically averaged from the WRF layer structure to a subset of CAMx layers when layer collapsing is specified by the user. Entrainment/detrainment profiles are adjusted to ensure that resultant vertical flux profiles within the cloud column go to zero at cloud top and at the ground. Finally, the units of entrainment/detrainment rates are converted to kg m^{-2} s^{-1}, and water/ice contents are converted to g/m^3 to be consistent with the grid-resolved cloud variables provided to CAMx. When these new KF variables are not available in the cloud/rain file, the CiG sub-grid cloud treatment is skipped in CAMx.

Most WRF output fields represent an instantaneous “snapshot” of the meteorological variables at each output time (usually the WRF output interval is hourly, but CAMx can read different WRF output frequencies). For this reason, many continuous state fields (thermodynamic variables, winds, mixing) are linearly interpolated to each CAMx time step between input/output intervals. This is difficult to do for discrete fields such as clouds, so historically cloud fields in CAMx have been held constant during each interval. This may alias the actual evolution of cloud fields occurring in WRF. Nonetheless, the sub-grid KF variables are also held constant in CAMx in each interval to stay consistent with grid-resolved cloud fields, thereby defining a steady-state CiG system during the interval. Time-averaging or time-interpolation between input/output intervals may be considered for future development.

2.1.2 The CAMx Cloud-in-Grid (CiG) System

Figure 2 presents a schematic illustration of a CiG cloud within a single CAMx grid column. Note that the CiG volume extends beyond the actual cloud volume (i.e., cloud base to cloud top) to include all contributing source layers below the cloud base. Vertical transport of constituents due to coupled convective dynamics between the CiG volume and the ambient grid column is defined from vertical integration of the input horizontal entrainment/detrainment flux profiles.

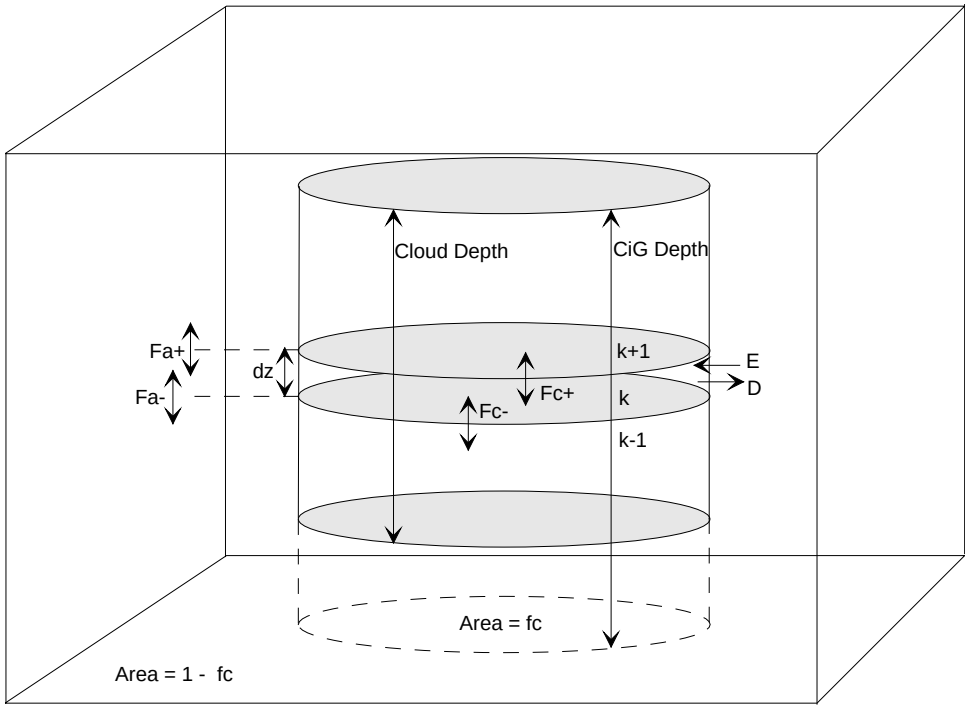

Figure 2. Schematic illustration of a CiG cloud within a single CAMx grid column, indicating grid, CiG and cloud volumes, area coverage and fluxes.

In an entraining/detraining cloud plume model, updraft and downdraft mass flux profiles (F_u, F_d) are balanced by lateral entrainment (E_u, E_d) and detrainment (D_u, D_d) fluxes in each layer (k) to maintain mass conservation:

$$F_u(k) - F_u(k-1) = E_u(k) - D_u(k)$$

$$F_d(k) - F_d(k-1) = E_d(k) - D_d(k)$$

All fluxes are in units of kg m^{-2} s^{-1}, which represents the amount of mass change per unit area of the grid column covered by the cloud. Vertical fluxes are staggered with respect to entrainment/detrainment fluxes, such that *F(k)* is assigned to the top of the layer, while *F(k-1)* is assigned to the bottom.

The CAMx CiG does not distinguish between separate updraft and downdraft fluxes, and instead assumes a well-mixed condition in each layer. It employs net entrainment/detrainment rates (E_c, D_c) and calculates a single net vertical flux (F_c) within the cloud:

$$E_c = E_u + E_d$$

$$D_c = D_u + D_d$$

$$F_c(k) - F_c(k-1) = E_c(k) - D_c(k)$$

We account for compensating vertical motions in the ambient portion of the grid column, adjusting for the fraction of cloud area (f_c) to ambient column area:

$$E_a = E_c\left(\frac{f_c}{1-f_c}\right)$$

$$D_a = D_c\left(\frac{f_c}{1-f_c}\right)$$

$$F_a(k) - F_a(k-1) = D_a(k) - E_a(k)$$

where E_a is the ambient entrainment flux to the cloud, D_a is the ambient detrainment flux from the cloud, and F_a is the vertical mass flux in the ambient.

The numerical solver for mass transport employs a first-order upstream approach. With potentially large vertical fluxes through thin layers, such explicit integration methods need to take small steps to remain stable and positive-definite. However, with time steps of possibly a few seconds and hundreds to thousands of chemical mass profiles on which to operate (including core model species and source apportionment tracers), an explicit solver applied to thousands of grid columns each hour would severely impact model speed. To address this issue we have developed an approach where, once each meteorological update time (usually 1 hour), the evolution of a single matrix of air mass tracer per convective column is solved for the duration of the local convective time scale. We then algebraically combine the final tracer matrix with every chemical profile in that column to yield the net effect of convective dynamics.

The air mass matrix is defined to represent the amount of mass that starts in a particular layer *l* and arrives at a particular layer *k* after the specified time interval. The mass is represented as a unitless mass mixing ratio, with an initial value of one along the matrix diagonal (1,1) $\rightarrow$(*N*,*N*), where *N* is the number of layers, and zero everywhere else. Because of very different vertical fluxes between the cloud and ambient columns, the evolution of four mass matrices are tracked: (1) mass starting in the cloud column and staying in the cloud column, (2) mass starting in the cloud column and detraining into the ambient column; (3) mass starting in the ambient column and staying the ambient column, and (4) mass starting in the ambient column and entraining into the cloud column. This results in the integration of $4 \times N$ individual tracers per grid column.

The evolution of each cloud mass element (M_{cc}) is calculated according to:

$$\Delta M_{cc}(l,k) = \frac{\Delta t}{\Delta z(k)\rho(k)}\left(F^- - F^+ + E_c(k)M_{ca}(l,k)\left(\frac{f_c}{1-f_c}\right) - D_c(k)M_{cc}(l,k)\right)$$

where Δt is timestep (s), Δz is layer depth (m), ρ is layer density (kg m^{-3}), and M_{ca} is previously detrained cloud mass that reenters via entrainment, accounting for the different fractional area of the ambient column. Employing an upstream differencing technique, the vertical interfacial

mass fluxes (F^+, F^-) are set according to their respective signs, e.g., for the in-cloud flux at the top of layer *k*:

$$F^+ = F_c(k)M_{cc}(l,k), \qquad F_c > 0$$

$$F^+ = F_c(k)M_{cc}(l,k+1), \quad F_c < 0$$

and for the in-cloud flux at the bottom of layer *k*:

$$F^- = F_c(k-1)M_{cc}(l,k-1), \quad F_c > 0$$

$$F^- = F_c(k-1)M_{cc}(l,k), \qquad F_c < 0$$

M_{ca} is similarly calculated with the exchange of mass from cloud to ambient:

$$\Delta M_{ca}(l,k) = \frac{\Delta t}{\Delta z(k)\rho(k)}\left(F^- - F^+ - E_c(k)M_{ca}(l,k) + D_c(k)M_{cc}(l,k)\left(\frac{1-f_c}{f_c}\right)\right)$$

Similar calculations are performed for the ambient mass elements (M_{aa}) and the mass entrained into the cloud (M_{ac}):

$$\Delta M_{aa}(l,k) = \frac{\Delta t}{\Delta z(k)\rho(k)}\left(F^- - F^+ - E_c(k)M_{aa}(l,k) + D_c(k)M_{ac}(l,k)\left(\frac{1-f_c}{f_c}\right)\right)$$

$$\Delta M_{ac}(l,k) = \frac{\Delta t}{\Delta z(k)\rho(k)}\left(F^- - F^+ + E_c(k)M_{aa}(l,k)\left(\frac{f_c}{1-f_c}\right) - D_c(k)M_{ac}(l,k)\right)$$

After integrating for a specified duration of time, the two final cloud mass matrices and the two final ambient mass matrices are stored for use until the next meteorological update time, at which point the process is repeated.

As CAMx marches forward during the interval between meteorological update times, it evolves the chemical fields in an operator splitting sequence that performs grid-resolved emissions, advection, diffusion, deposition, and chemistry. The new CiG algorithm is placed within this sequence just before chemistry. First, CiG performs convective transport adjustments by multiplying each species (*i*) concentration profile (C^i, in the internal units of mass/volume) into the ambient and cloud mass matrices, yielding new transport-adjusted ambient and cloud profiles:

$$C_c^i(k) = \sum_{l=1,N}\left[C^i(l)M_{cc}(l,k) + C^i(l)M_{ac}(l,k)\left(\frac{1-f_c}{f_c}\right)\right]$$

$$C_a^i(k) = \sum_{l=1,N}\left[C^i(l)M_{aa}(l,k) + C^i(l)M_{ca}(l,k)\left(\frac{f_c}{1-f_c}\right)\right]$$

where again *l* is the source layer and *k* is the arrival layer. Then CiG performs aqueous chemistry and wet scavenging separately on the in-cloud and ambient concentration profiles according to resolved and sub-grid cloud and precipitation inputs. Finally, the two chemical profiles are linearly combined to yield the net result of cloud/ambient transport, chemistry, and wet removal on the given profile:

$$C^i = f_c C_c^i + (1 - f_c) C_a^i$$

This process has been rigorously checked to ensure that all mass matrices and their application to chemical concentration profiles conserve mass to within 6 significant figures.

Gas-phase chemistry and PM thermodynamic equilibrium require the largest amount of computing time among all processes. To minimize runtime impacts with the introduction of the CiG, both of these processes continue to operate on the single total column chemical profiles as the last step in the operator splitting sequence, after the CiG processes are completed. Photolysis rates are adjusted by the effects of all resolved and sub-grid clouds in the column using the same cloud optical depth algorithm as in previous versions (Emery et al., 2010), calculated by WRFCAMx and passed to CAMx via the cloud/rain input file. Photolysis rates are also adjusted for PM turbidity using the same aerosol optical depth algorithm within CAMx as in previous versions (ENVIRON, 2014).

This CiG implementation is not the only possible scheme that could be driven by the KF convective parameterization. An important assumption is that a grid cell contains two well-mixed air volumes: in-cloud air and ambient air. A more general approach would treat three separate volumes: in-cloud updraft air, in-cloud downdraft air, and ambient air. The two-volume implementation is equivalent to a three-volume implementation with highly-efficient mixing among the two in-cloud parcels. A three-volume CiG could be developed with in-cloud interactions controlled by a mixing coefficient. Such an implementation would require additional internal memory and more than twice the computing time for the CiG calculations, and it is not clear how to parameterize the in-cloud mixing coefficient other than to tune it against observations. Tuning would require several well-modeled convective cases with corresponding observations, none of which are available during DISCOVER-AQ or START-08.

2.2 Preliminary Testing

2.2.1 1-D Transport Process Testing

A one-dimensional convective mixing test bed program was constructed that allowed us to: (1) demonstrate the approach as a proof-of-concept; and (2) develop details of the technical design, refine the approach, and perform quality assurance (QA) checks in the coding of the transport solver (detailed in Section 4). The transport equations and tracer matrices described in Section 2.1.2 were coded into a Fortran subroutine that was directly incorporated into CAMx after this preliminary testing phase. Reasonably representative profiles of convective entrainment/ detrainment fluxes and initial tracer concentrations were specified for a vertical

column resolved into 20 layers. Vertical fluxes were calculated from the entrainment/detrainment fluxes, from which vertical tracer transport and exchange between in-cloud and ambient fractions of the grid column were determined. The test bed integrated tracer transport over 1 hour. Mass conservation for the transport matrices and the tracer profile was met to within 6 significant figures during the 1 hour integration.

Figure 3 shows the net entrainment/detrainment and vertical flux profiles used for testing. Profiles are designed to represent a deep yet moderately convective cloud spanning 1 to 9 km while horizontally occupying 30% of the column. Figure 4 shows the initial and final tracer concentration profiles. The initial tracer (blue) represents a pollutant profile typical of late morning, with highest concentrations in the boundary layer and a strong gradient aloft decaying to 1% of the surface value. The initial profile is assigned equally to the ambient and in-cloud portion of the column at the start of integration, and then allowed to evolve separately (dashed lines) for 1 hour, leading to a final combined profile (red). The final profile accounts for in-cloud upward transport, ambient downward subsidence, and the exchange between the two. The net effect is a large increase in mid- and upper-tropospheric concentrations at the expense of boundary layer and low-tropospheric concentrations. This pattern is consistent with expectations.

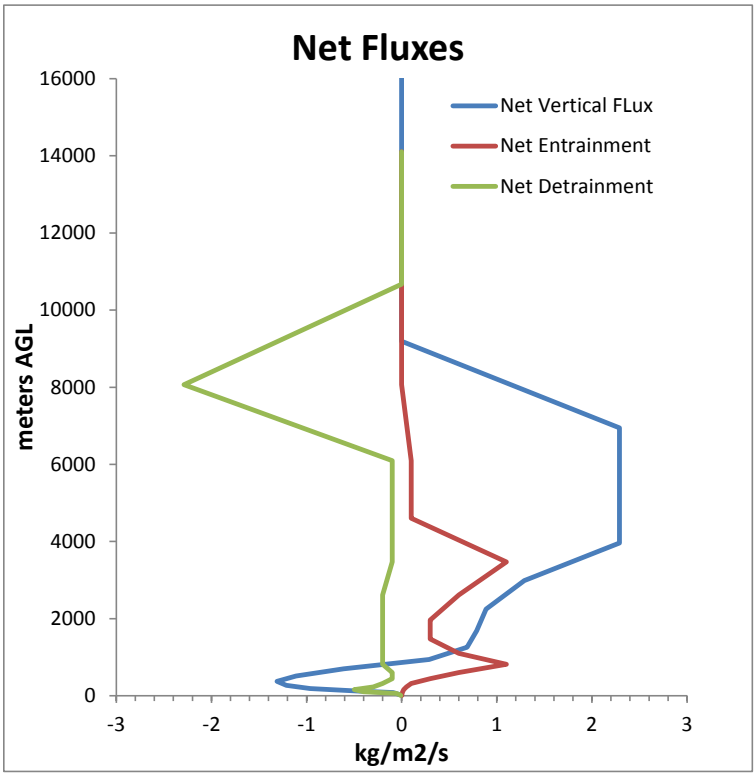

Figure 3. Net convective entrainment/detrainment and vertical mass fluxes specified for the test bed proof-of-concept case.

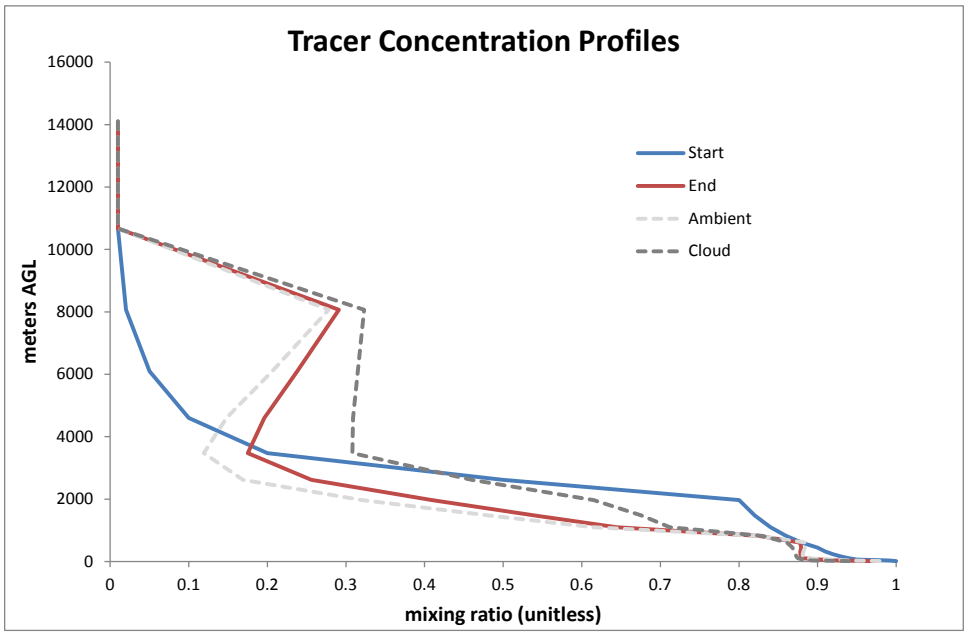

Figure 4. Initial and final tracer concentration profiles after 1 hour of convective transport.

2.2.2 Testing WRF and WRFCAMx Interface Updates

Preliminary testing was conducted using WRF v3.6.1, which was released by NCAR in late 2014 and includes the RadKF radiation feedback implemented by Alapaty et al. (2012). WRF was run for a week-long period in June 2013 on a single 36 km grid. The model configuration was set according to previous projects conducted for TCEQ (Kemball-Cook et al., 2014b; Johnson et al., 2013, 2015); details are given in Section 3.1.

WRFCAMx processed output from the WRF run in 3 ways: (1) only WRF-resolved cloud data were used to generate total cloud field inputs for CAMx; (2) the original WRFCAMx approach to diagnose sub-grid clouds was used to generate total cloud field inputs for CAMx; (3) the new WRFCAMx KF sub-grid cloud option was used to generate separate resolved and sub-grid cloud inputs for CAMx. Both sub-grid cloud cases included the diagnosis of sub-grid stratiform clouds according to the original approach in WRFCAMx (Emery et al., 2010).

QA checks were performed to ensure that new code was correctly implemented and was properly processing new cloud data and generating the CAMx data files (see Section 4). These QA steps revealed certain aspects of the technique that required slight modifications to a few details, and also revealed issues in the original diagnostic option that led us to improve the robustness of that approach as well. WRFCAMx speed was not impacted by the additional of the KF option or by any subsequent modifications from the QA procedures.

Figure 5 shows the GOES[2]-East visible image of the eastern US at 2215 UTC (4:15 PM CST) on June 22, 2013. Figure 6 displays resulting CAMx-ready input total (resolved + sub-grid) cloud fields, expressed as vertically-integrated cloud opacity (i.e., optical depth), for the three test cases at 4:00 PM CST. The resolved-only cloud case clearly lacks cloud coverage. The sub-grid cloud cases exhibit a more expected cloud pattern and coverage that agree better with the satellite image. The diagnosed and KF sub-grid cloud fields are more similar than different, although the diagnosed case exhibits slightly more cloud coverage, particularly over the Atlantic Ocean where KF agrees better with satellite image. The QA review confirmed that these differences are the direct result of the different methodologies as opposed to coding errors.

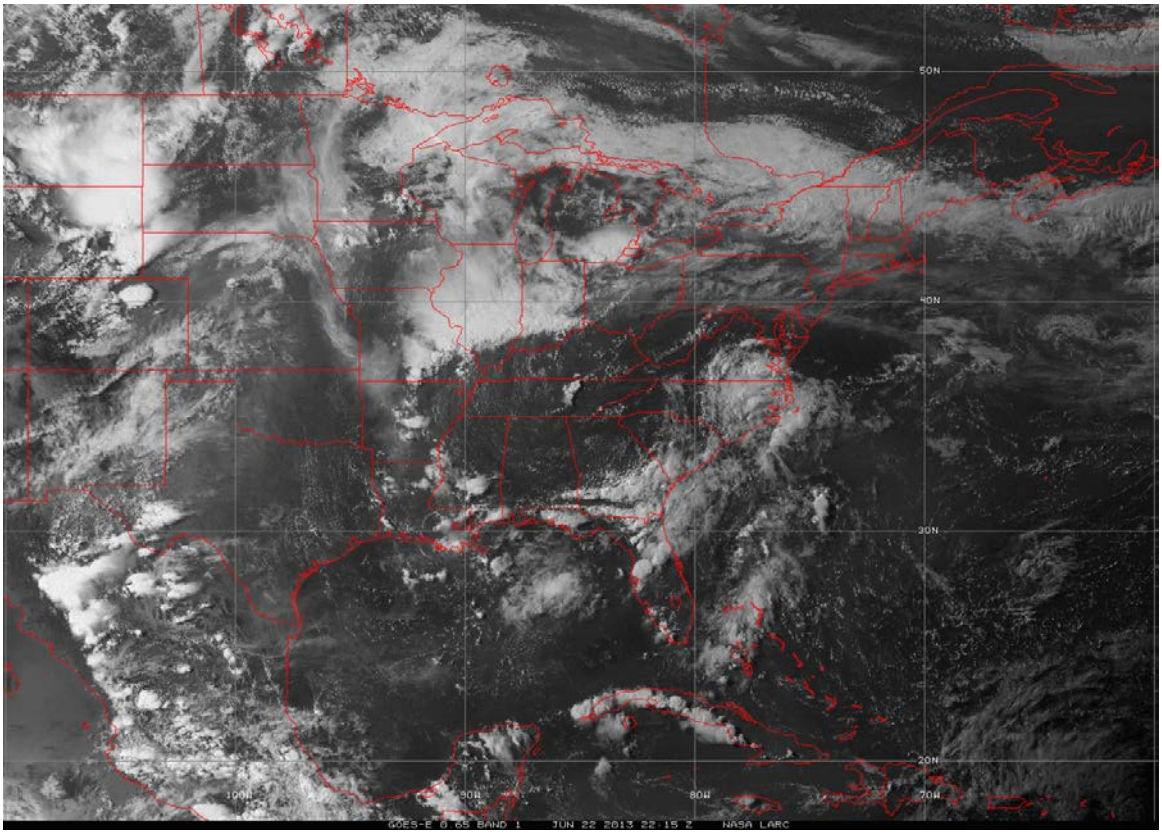

Figure 5. GOES[2]-East visible satellite image of the eastern US at 2215 UTC (4:15 PM CST) on June 22, 2013.

[2] Geostationary Operational Environmental Satellite (GOES), operated by the National Oceanic and Atmospheric Administration (NOAA).

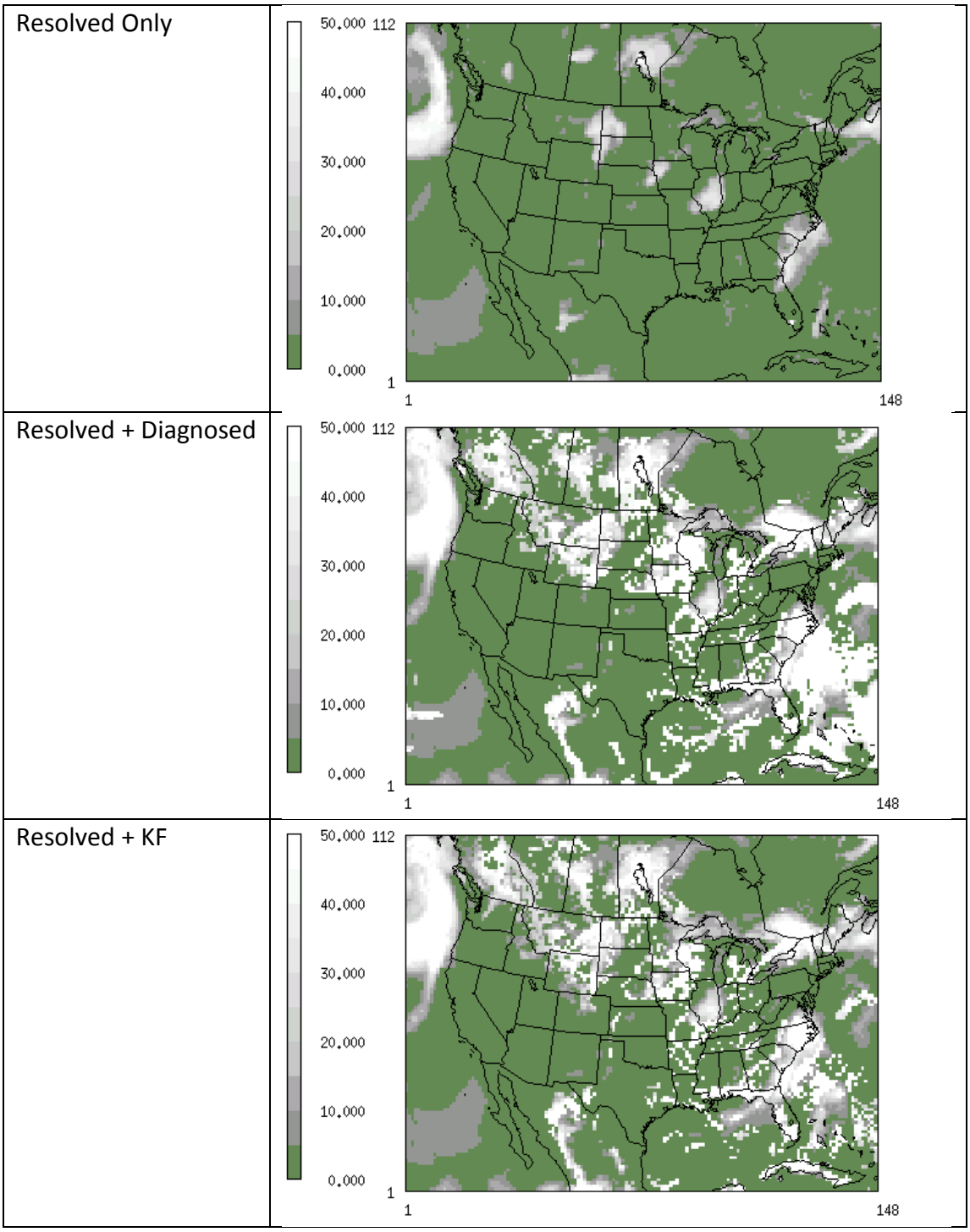

Figure 6. CAMx-ready input total cloud fields (expressed as unitless optical depth) for three test cases at 4:00 PM CST on June 22, 2013. (Top) resolved clouds only; (middle) resolved plus diagnosed sub-grid clouds; (bottom) resolved plus KF sub-grid clouds.

2.2.3 CAMx CiG Testing

The convective transport algorithm described in Sections 2.1.2 and 2.2.1 was implemented into CAMx v6.10. CAMx was run for two days in June 2013 on a single 36 km grid, driven by meteorological fields as described in Section 2.2.2. The CAMx model configuration, emissions, and initial/boundary conditions were taken from previous projects conducted for TCEQ (Kemball-Cook et al., 2014b; Johnson et al.., 2013; 2015). CAMx was run in 3 modes: (1) original unmodified CAMx v6.10; (2) modified CAMx with the CiG option turned off to emulate the original model; and (3) modified CAMx with the CiG option turned on.

Extensive QA testing was conducted to ensure that new code was correctly implemented and was properly processing convective transport, wet scavenging, and aqueous chemistry (see Section 4). Particular attention was given to mass conservative and positive-definite solutions, both of which were achieved. These QA steps revealed certain aspects of the technique that required modifications to a few details. Tests with the original version of CAMx and the new version with CiG turned off correctly resulted in identical output fields.

CAMx with CiG was also tested with various parallelization techniques: (1) no parallelization; (2) Open Multi-Processor (OMP) shared-memory parallelization; and (3) Message Passing Interface (MPI) distributed-memory parallelization. CAMx tests for both single processor and OMP parallelization across 8 processors achieved identical results, while OMP speed improvements were consistent with the original CAMx code. Testing with MPI parallelization resulted in minor differences from the single-processor and OMP cases. This was tracked to an area of the code that was not related to the new CiG implementation (a problem in the original code), which when identified was easily fixed and subsequent MPI results aligned exactly with OMP and single-processor results. MPI speed improvements were found to be consistent with the original CAMx code.

Figure 7 displays resulting CAMx output fields for NO_2 and ozone at two levels (surface layer and layer 26 – about 8 km aloft) at 4:00 PM CST on June 22, 2013. Results are shown for CAMx without CiG invoked, and the differences in concentrations resulting from invoking the CiG. At the surface, effects from CiG on NO_2 and ozone are relatively small at this hour, with NO_2 differences within 10 ppt and ozone differences within 1 ppb. Aloft, effects from CiG are larger relative to the no-CiG concentrations, with NO_2 differences within 30 ppt and ozone differences extending to 25 ppb. The effects of vertical convection indicate both upward and downward transport. For example, where ozone aloft is high (i.e., around British Columbia) convection brings ozone down to increase surface concentrations; in the central US where surface ozone is high, convection reduces surface concentrations and increases concentrations aloft. Results include the mitigating effects of wet scavenging in precipitating convection.

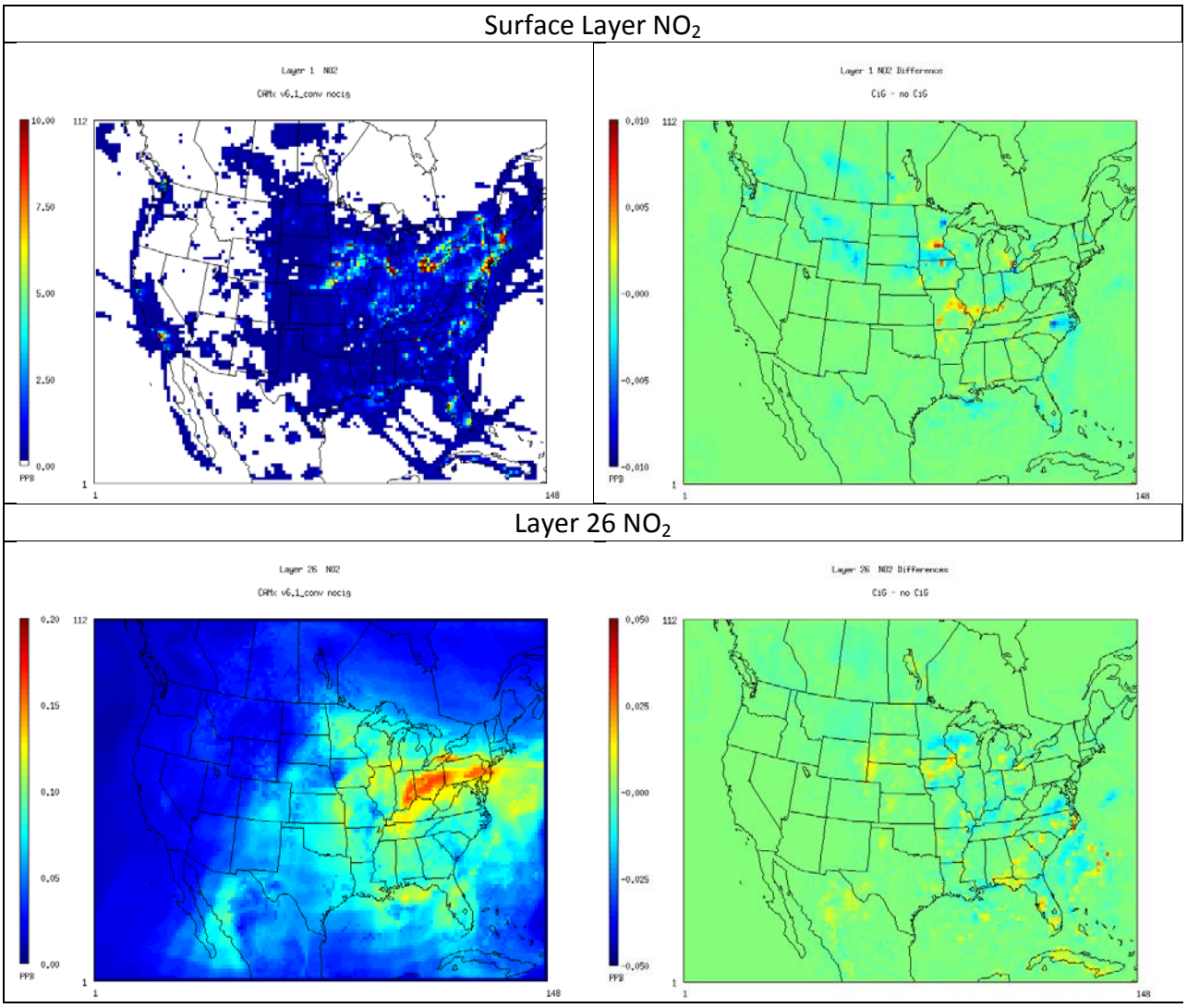

Figure 7(a). CAMx output fields of NO_2 at 4:00 PM CST on June 22, 2013. Total concentrations from CAMx without CiG invoked are shown on the left, differences in concentrations resulting from invoking CiG are shown on the right. The top row shows effects in the surface layer, the bottom row shows effects in layer 26 (about 8 km above the surface).

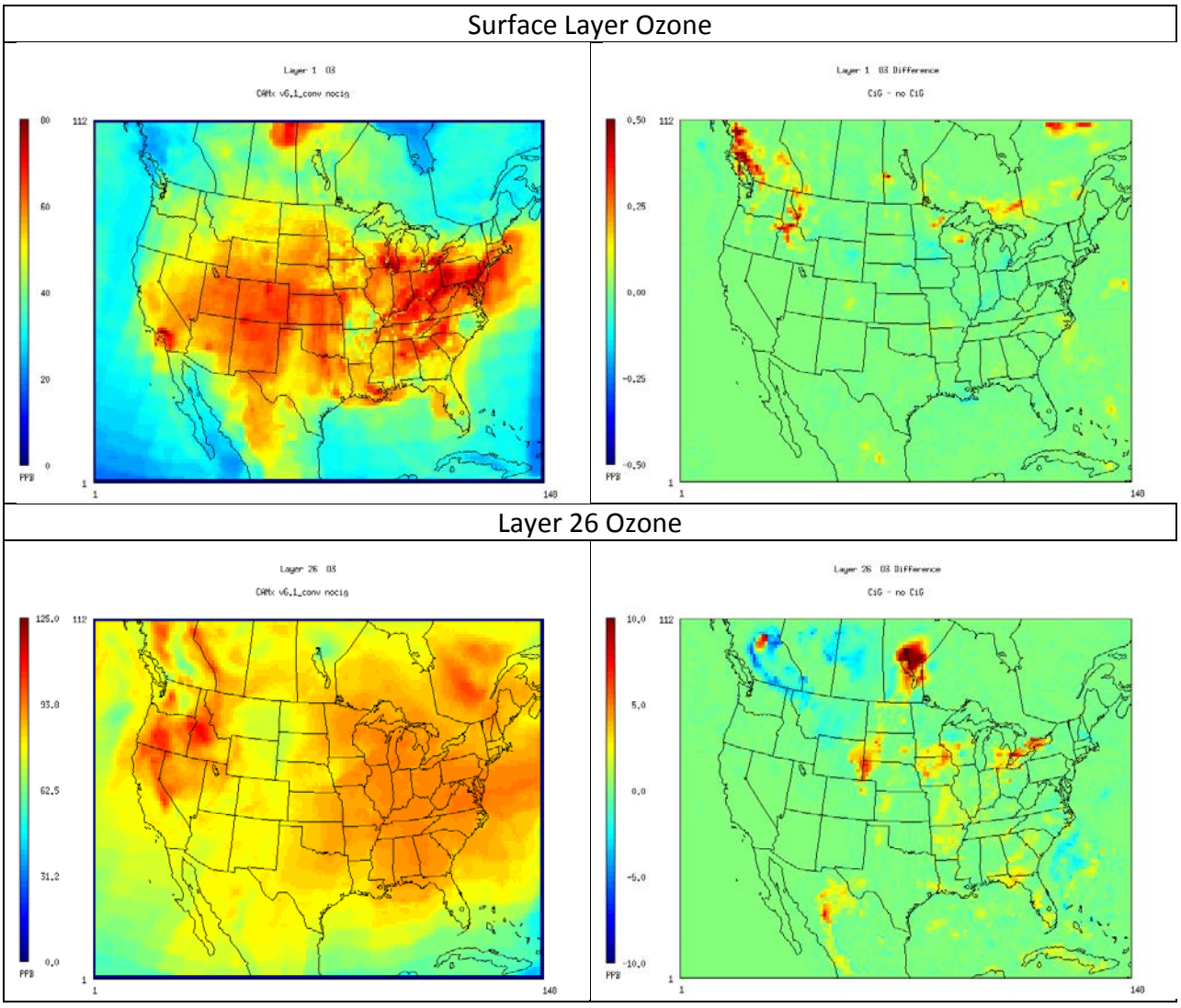

Figure 7(b). CAMx output fields of ozone at 4:00 PM CST on June 22, 2013. Total concentrations from CAMx without CiG invoked are shown on the left, differences in concentrations resulting from invoking CiG are shown on the right. The top row shows effects in the surface layer, the bottom row shows effects in layer 26 (about 8 km above the surface).

3.0 APPLICATION AND EVALUATION

Ramboll Environ and TAMU ran WRF with NERL's KF updates for two test cases. The cases were selected for their variety of convective modes and the availability of measurements in the boundary layer and free troposphere. WRF output from each case was passed through the updated WRFCAMx interface program, and CAMx with CiG was run using pre-existing emissions and ancillary input datasets.

The project team conducted a qualitative evaluation of CAMx results against ambient measurements. The team developed graphical products with which to facilitate the evaluation, specifically including *in situ* concentration measurements from the DISCOVER-AQ and START08 databases. The team collaborated on evaluating these products and identifying any clear problems in the modeling results. Particular focus was placed on how well CAMx captures or evolves features in the profiles of NOx, ozone and CO during monitored convective periods, and how the WRF/CAMx modeling system qualitatively performs overall in characterizing convection and its impacts to spatial and temporal pollutant distributions.

3.1 September 2013 DISCOVER-AQ

The first case covered September 1-8, 2013 during early DISCOVER-AQ operations around Houston (Pickering et al., 2013); particularly on September 4-6, substantial shallow and deep convection developed and moved across the Houston area. One particular aircraft (NASA P-3) sampled vertical columns up to 3-5 km at several locations in the Houston-Galveston area before and after the scattered deep convection moved through the area. Flight paths are shown in Figure 8.

Ramboll Environ obtained the public release of WRF v3.6.1 (containing the RadKF treatment) in late 2014, and WRF v3.7 (containing the MSKF treatment) in April 2015. We implemented additional code modifications in both WRF versions to output convective fluxes and time scale variables needed to drive the CAMx CiG model. We tested both versions to ensure that they ran properly without errors and crashes. WRF v3.7 was run for the September 2013 case, while WRF v3.6.1 was run for both 2013 and 2008 cases.

WRF v3.6.1 (using RadKF) and v3.7 (using MSKF) were run for September 1-8, 2013 on the 36 and 12 km nested grids shown in Figure 9. WRF was configured to be consistent with the layer structure (Figure 10), physics options, and data assimilation inputs and specifications employed by Kemball-Cook et al. (2014b) and Johnson et al. (2013, 2015). Since RadKF should not be applied at scales smaller than ~10 km, we excluded the 4 km grid in these analyses so that RadKF and MSKF could be run and compared on consistent grid configurations to support the CAMx CiG evaluation. Table 1 lists the specific WRF configuration used for the September 2013 testing simulations; model inputs and configurations were identical for both versions of WRF except for the choice of the cumulus scheme. This same configuration was applied in the preliminary testing of CAMx/CiG during a June 2013 episode, as described in Section 2.2.

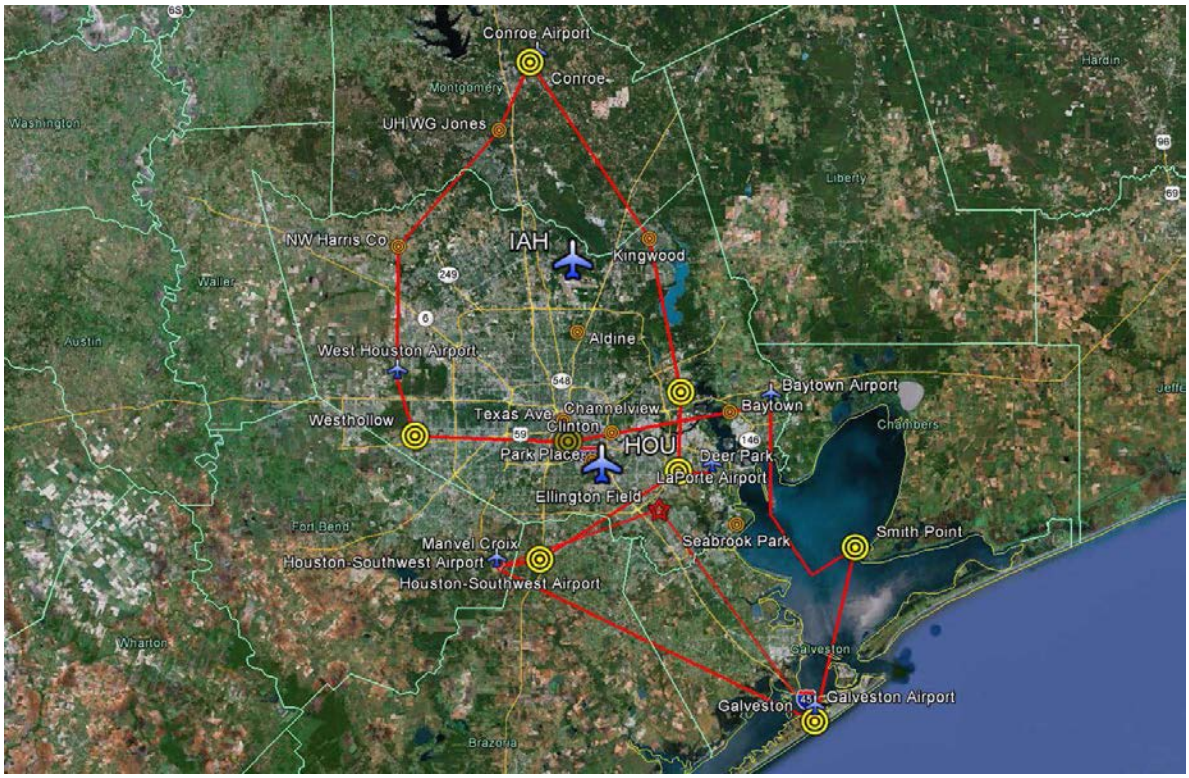

Figure 8. P-3 aircraft flight paths during 2013 Texas DISCOVER-AQ (Pickering, 2013). Spiral profiles are denoted by yellow circles.

Figure 9. WRF modeling domains at 36-km grid spacing (red) and 12-km spacing (dark blue), and corresponding CAMx domains at 36-km spacing (gray) and 12-km spacing (light blue). http://www.tceq.texas.gov/airquality/airmod/rider8/modeling/domain.

Vertical Layer Structure

Corresponding WRF Layer	Layer Top (m AGL)	CAMx Layer	Layer Center (m AGL)	Thickness (m)
38	15179.1	28	13637.9	3082.5
36	12096.6	27	10631.6	2930.0
32	9166.6	26	8063.8	2205.7
29	6960.9	25	6398.4	1125.0
27	5835.9	24	5367.0	937.9
25	4898.0	23	4502.2	791.6
23	4106.4	22	3739.9	733.0
21	3373.5	21	3199.9	347.2
20	3026.3	20	2858.3	335.9
19	2690.4	19	2528.3	324.3
18	2366.1	18	2234.7	262.8
17	2103.3	17	1975.2	256.2
16	1847.2	16	1722.2	249.9
15	1597.3	15	1475.3	243.9
14	1353.4	14	1281.6	143.6
13	1209.8	13	1139.0	141.6
12	1068.2	12	998.3	139.7
11	928.5	11	859.5	137.8
10	790.6	10	745.2	90.9
9	699.7	9	654.7	90.1
8	609.7	8	565.0	89.3
7	520.3	7	476.1	88.5
6	431.8	6	387.9	87.8
5	344.0	5	300.5	87.1
4	256.9	4	213.8	86.3
3	170.6	3	127.8	85.6
2	85.0	2	59.4	51.0
1	33.9	1	17.0	33.9

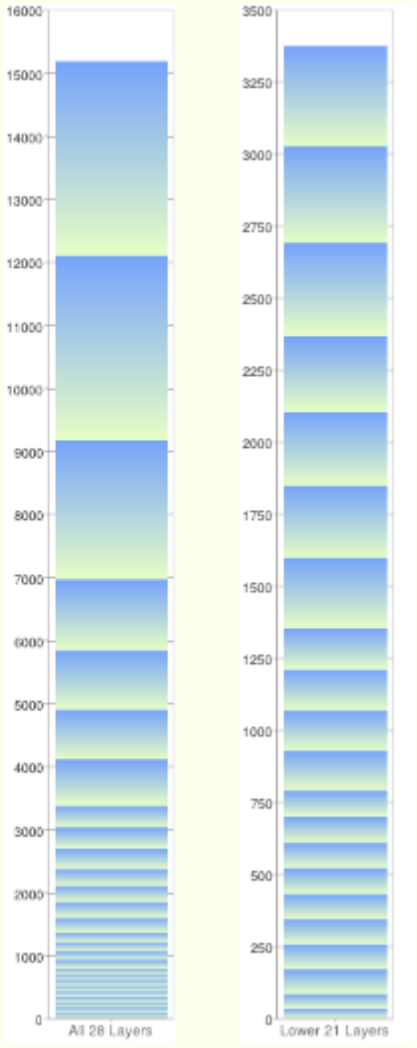

AGL - Above Ground Level.

Figure 10. Mapping between WRF and CAMx model vertical layer structures for the September 2013 DISCOVER-AQ period. The WRF domain extends to ~20 km (50 hPa) with 43 layers. http://www.tceq.texas.gov/airquality/airmod/rider8/modeling/domain.

Table 1. WRF physics configuration for the June and September 2013 simulations.

WRF Physics Option	Option Selected	Notes
Cloud Microphysics	WRF Single-Moment 6-class (WSM6)	A scheme with ice, snow and graupel processes suitable for high-resolution simulations.
Longwave and Shortwave Radiation	RRTMG	Rapid Radiative Transfer Model for General Circulation Models (GCM); an accurate scheme using look-up tables for efficiency; accounts for multiple bands, and microphysics species.
Surface Layer Physics	MM5 similarity	Based on Monin-Obukhov with Carslon-Boland viscous sub-layer and standard similarity functions from look-up tables; adopted from the 5th Generation Mesoscale Model (MM5).
Land Surface Model	Noah	NCEP/NCAR land surface model with soil temperature and moisture in four layers, fractional snow cover and frozen soil physics.
PBL Scheme	Yonsei University (YSU)	Non-local-K scheme with explicit entrainment layer and parabolic K profile in unstable mixed layer.
Cumulus Parameterization	Kain-Fritsch	Deep and shallow convection sub-grid scheme using a mass flux approach with downdrafts and CAPE removal time scale; modified by EPA/NERL to include cloud feedback to RRTMG radiation scheme (RadKF in v3.6.1) and to extend applicability to smaller scales (MSKF in v3.7).
Initial/Boundary Conditions and Analysis Nudging	12 km North American Model (NAM) Analyses	Applied on both 36 and 12 km grids; no observational nudging was applied.

CAMx was run using pre-existing datasets developed by Ramboll Environ and TCEQ during several current and past projects conducted for the State of Texas (e.g., Kemball-Cook et al., 2014b). This case allowed us to examine CAMx performance in the context of the complex emissions matrix of the Houston-Galveston airshed. Figure 9 presents the 36/12 km CAMx modeling domains. Figure 10 displays how 38 WRF layers (of 43 total) collapse to 28 CAMx layers. The CAMx inputs for the September 2013 case included:

- Initial and boundary conditions extracted from 2013 day-specific 6-hourly output from the Model for OZone And Related chemical Tracers (MOZART; https://www2.acd.ucar.edu/gcm/mozart), with certain modifications to reduce unrealistically high ozone on south/east boundaries and to reduce unrealistic contributions from Canadian wildfires;
- Mix of 2012 and 2013 elevated point source emissions provided by TCEQ during 2014-2015;
- 2012 low-level anthropogenic emissions (area, mobile, etc.) by day type (weekday, Friday, Saturday, Sunday) provided by TCEQ;
- Biogenic emissions from the Model of Emissions of Gases and Aerosols from Nature (MEGAN) v2.10, derived from pre-existing WRF runs that also employed the RadKF modifications by Alapaty (2012);
- Fire emission from 2013 day-specific data from the Fire INventory from NCAR (FINN; https://www2.acd.ucar.edu/modeling/finn-fire-inventory-ncar);

- YSU vertical diffusivity (Kv) fields derived using WRFCAMx, without landuse-based Kv modifications (or "patching");
- Day-specific column ozone and photolysis rates inputs derived from 1 degree Total Ozone Mapping Spectrometer (TOMS) satellite ozone column data;
- Gridded landuse and leaf area index (LAI) inputs from datasets derived from the Moderate-resolution Imaging Spectroradiometer (MODIS) satellite data.

Modeling did not include aircraft emissions at cruise altitude (i.e., in upper troposphere and lower stratosphere) or lightning NOx as developed by Kemball-Cook et al. (2013). Modeling also did not include explicit top boundary conditions now available in CAMx v6.20 that can be derived from GEOS-Chem or MOZART global chemistry models (Kemball-Cook et al., 2014a).

3.2 May 2008 START08

The second case was run during a week-long period during the Stratosphere-Troposphere Analyses of Regional Transport 2008 (START08; Pan et al., 2010). START08 was designed to measure the effects of a wide variety of transport and mixing processes in the upper troposphere and lower stratosphere, including deep convection. The key platform for START08 was an NCAR Gulfstream-V aircraft equipped with sensors measuring ozone (O_3), carbon monoxide (CO), carbon dioxide (CO_2), nitric oxide (NO), NOy, methane (CH_4), nitrous oxide (N_2O) and 55 other trace species. High-altitude and vertical column measurements were made within a triangle bounded by Colorado, the northern Gulf of Mexico, and Missouri. TAMU previously simulated a May 6, 2008 case with WRF to study the transport effects of explicitly-resolved convection (Siu et al., 2015). This period featured a fast-moving squall line over North Texas and associated convective systems in Oklahoma. A second case occurred on June 16, 2008, which was an instance of unorganized, diurnally-forced deep convection over the south-central United States. However, this case was dropped from consideration in this project as WRF could not sufficiently replicate locations and timing of convection for any of multiple model configurations.

WRF v3.6.1 was run for the May 1-8, 2008 START08 episode for 36 and 12 km nested grids that align with, and are slightly larger than, the CAMx 36 and 12 km grids shown in Figure 11. WRF was configured to be consistent with the physics options and data assimilation inputs and specifications from Kemball-Cook et al. (2014b) and Johnson et al. (2013, 2015) as described in Table 1. The WRF and CAMx layer structures (Table 2) were configured to support an existing 2008 CAMx modeling database developed by Alpine Geophysics (described below). The RadKF cumulus parameterization of Alapaty et al. (2012) was used to support the CAMx convection model.

The team employed an existing 2008 CAMx modeling dataset that was used in two prior AQRP projects (Emery et al., 2013b; McDonald-Buller et al., 2013). This dataset was developed by Alpine Geophysics for the Houston Eight Hour Ozone Coalition (a cooperative of Houston petrochemical and refining companies). This dataset was developed for a continental US

(CONUS) 36 km grid, a large 12 km nested grid over the central US, and a local 4 km nested grid over Houston (Figure 11). The CAMx vertical grid consisted of 30 of the original 43 WRF vertical layers (Table 2). Emissions included both ozone and PM precursors chemically speciated for the CB05 chemical mechanism, based on data from both the TCEQ and EPA (Table 3). Biogenic emissions were available from both MEGAN and the Global Biosphere Emissions and Interactions System (GloBEIS), but only GloBEIS emissions were used in this project. The 36 and 12 km CAMx grids were run in 2-way interactive nested mode; the 4-km grid shown in Figure 11 was not used. Boundary conditions were developed for the 36 km CONUS grid using 6-hourly output from the MOZART global model (Emery et al., 2013b). Similarly to the September 2013 case, modeling did not include aircraft emissions at cruise altitude, lightning NOx, or explicit top boundary conditions.

Table 2. Mapping between WRF and CAMx model vertical layer structures for the May 2008 episode.

WRF Layer	Sigma	CAMx Layer	P (mb)	Layer Top (m AGL)	Layer Center (m AGL)	Thickness (m)
43	0.000	30	50	18872	18019	1707
41	0.025	29	74	17165	15608	3115
38	0.090	28	136	14050	12669	2762
35	0.175	27	216	11288	9949	2678
32	0.290	26	326	8610	7588	2044
29	0.405	25	435	6566	6041	1050
27	0.475	24	501	5516	5077	879
25	0.540	23	563	4637	4265	745
23	0.600	22	620	3893	3547	691
21	0.660	21	677	3202	3038	328
20	0.690	20	706	2874	2715	317
19	0.720	19	734	2556	2403	307
18	0.750	18	763	2249	2125	249
17	0.775	17	786	2000	1879	243
16	0.800	16	810	1757	1639	237
15	0.825	15	834	1520	1404	232
14	0.850	14	858	1288	1220	136
13	0.865	13	872	1152	1085	135
12	0.880	12	886	1017	951	133
11	0.895	11	900	884	819	131
10	0.910	10	915	753	710	86
9	0.920	9	924	667	624	86
8	0.930	8	934	581	538	85
7	0.940	7	943	496	454	84
6	0.950	6	953	412	370	84
5	0.960	5	962	328	286	83
4	0.970	4	972	245	204	82
3	0.980	3	981	163	122	82
2	0.990	2	991	81	57	49
1	0.996	1	996	32	16	32

Table 3. Configuration and input data for the 2008 CAMx modeling system developed by Alpine Geophysics and employed in previous AQRP projects (Emery et al., 2013b; McDonald-Buller et al., 2013).

Model Component	Description
Modeling Period	April 1 - October 18, 2008
Modeling Domain	36/12/4 km
Vertical Structure	30 Layers
Meteorological Model	WRF
Chemical Mechanism	Carbon Bond 2005 (CB05)
Boundary Conditions	MOZART
Deposition	Zhang
Emissions	
• Biogenics	MEGAN and GloBEIS
• On-road Motor Vehicles	MOVES
• Off-Road Motor Vehicles	EPA NEI*
• Shipping	EPA NEI*
• Area Source	EPA NEI*
• Point Source	TCEQ
• Wild Fire	BlueSky/EPA SMARTFIRE 2

*US National Emission Inventory, compiled by the US EPA.

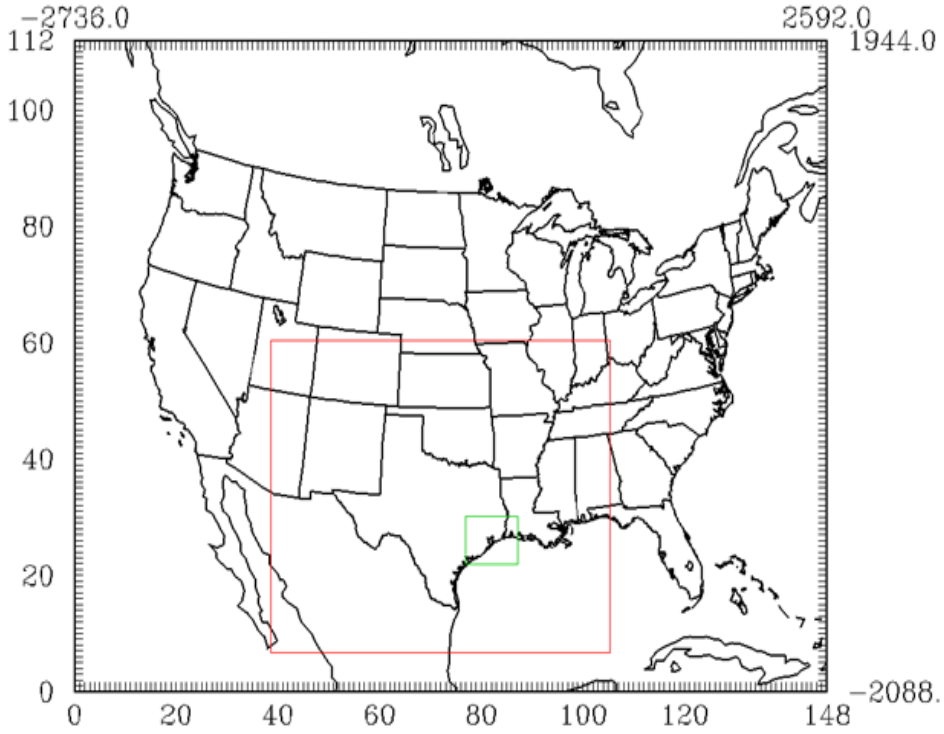

Figure 11. CAMx modeling grids developed by Alpine Geophysics for the 2008 modeling application: outer 36 km grid (full extent of map), 12 km nest (red), 4 km nest (green; not used).

3.3 Analyses and Evaluation

The quality of the WRF simulations was determined by a qualitative comparison of the simulated and observed radar reflectivity and surface rainfall fields as a function of space and time. The WRF simulations tended to underestimate the amount of convection in the areas sampled by aircraft. In an attempt to create a WRF simulation that was more consistent with observations, approximately 80 WRF runs were performed using different model initialization times, different nudging configurations, different nesting interaction levels, different combinations of microphysics and boundary layer schemes, and different convective triggers within the KF scheme. Using a longer spin-up time and a different convective trigger produced the best results for the May 2008 case but did not substantially improve the September 2013 case.

We first ran WRF with the initial physics configuration (Table 1), but it did not produce a realistic simulation, so we experimented with different combinations of microphysical and surface layer similarity schemes. The microphysical schemes that we tested include: WRF Double-Moment 6-class, Lin et al., Goddard GCE, Thompson graupel, and Morrison 2-moment schemes. The surface layer schemes we tested include the Eta similarity and TEMF schemes. However, none of these tests improved the simulation, so we kept the original configuration (WRF Single-Moment 6-class microphysics and MM5 Surface Layer Physics). We then tried different nesting interaction levels and convective triggers within the KF scheme. We found that a combination of two-way nested interaction and the moisture-advection modulated trigger function performed much better than the original one-way nested run and the default KF trigger. Originally we initialized WRF 6-12 hours before the genesis of the convective systems to allow enough time for the spin-up of the relevant physics. Since the CAMx chemical simulation needs a much longer time to spin up, we moved the model start time back in time by five days. In order to reduce WRF model drift from observed conditions, we added analysis nudging for the first 84 hours in both domains then turned it off for the remainder of the simulation so that it would not suppress convection.

3.3.1 September 2013

Local convective activity developed across Texas during the first 5-6 days of September, particularly along the Gulf Coast, which propagated from east to west each day. Figure 12 shows WRF-generated total cloud fields on the 12 km grid at 3 PM CST September 4 for three cases: (1) resolved clouds from WRF v3.6.1 plus diagnosed sub-grid clouds using the original WRFCAMx interface technique; (2) resolved plus RadKF clouds from WRF v3.6.1; and (3) resolved plus MSKF clouds from WRF v3.7. Figures 13 and 14 present weather charts and satellite imagery at about the same time. Note that WRF v3.7 more correctly generates convection over southeast Texas on September 4, while WRF v3.6.1 shifts the convective band too far south. Although actual convective activity continued through September 5-6, both versions of WRF do not exhibit sufficient convection on these later days (not shown).

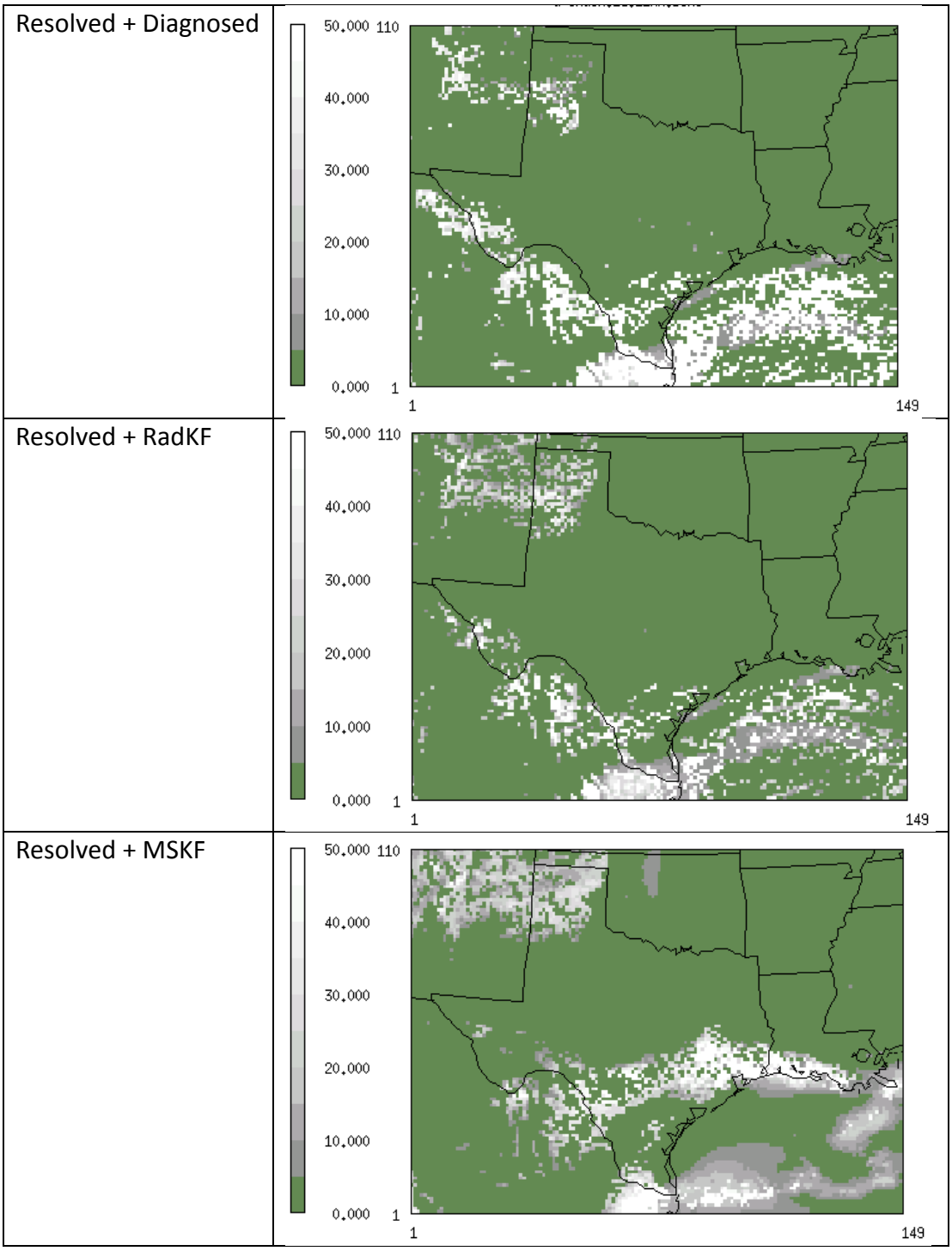

Figure 12. CAMx-ready input total cloud fields (expressed as unitless optical depth) on the 12 km grid for three cases at 3 PM CST, September 4, 2013. (Top) resolved plus diagnosed sub-grid clouds; (middle) resolved plus RadKF sub-grid clouds; (bottom) resolved plus MSKF sub-grid clouds.

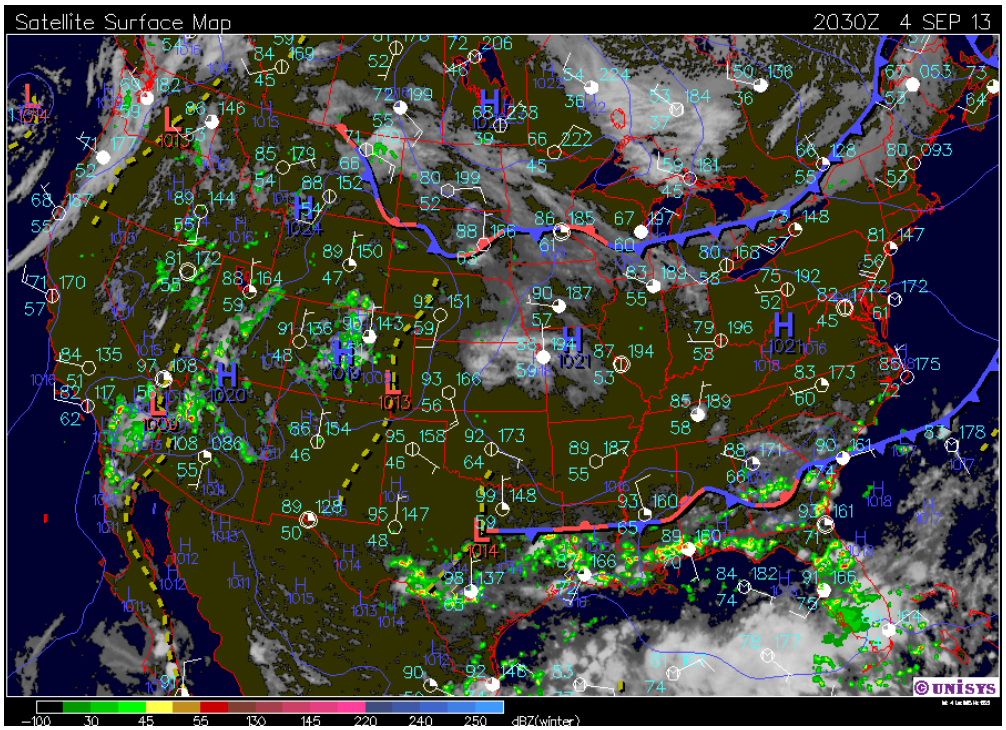

Figure 13. Composite satellite weather chart at 2:30 PM CST, September 4, 2013.

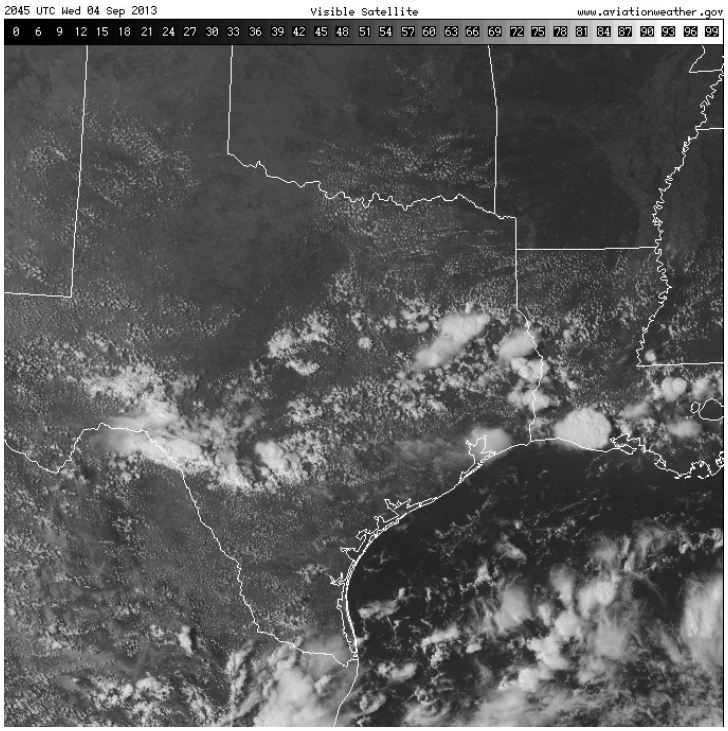

Figure 14. Visible satellite image at 2:45 PM CST, September 4, 2013.

Aside from cloud patterns, these two WRF simulations result in fundamentally different meteorological patterns that impact the CAMx ozone simulations, despite otherwise identical configurations and inputs. Figure 15 shows ozone differences between CAMx/CiG using WRF v3.7/MSKF meteorology and WRF v3.6.1/RadKF meteorology on the afternoon of September 4 (consistent with Figures 13 and 14). Surprisingly large and widespread differences in ozone are evident across the 12 km grid, with particularly large ozone decrements in the MSKF case that approach 50 ppb along the Gulf coast of southern Texas. In that area, the RadKF case results in ozone ranging 70-90 ppb, but MSKF results in ozone of about 40 ppb where measurements in the Corpus Christi-Victoria area peak at 37 ppb. It is not clear whether differences in other areas of the domain are purely the result of different cumulus schemes in combination with CAMx CiG, or if other changes implemented in WRF v3.7 affect various aspects of transport, mixing and chemistry in the photochemical model. Nevertheless, with its better ozone simulation along the Gulf Coast, we focus the evaluation of CAMx/CiG on the MSKF simulation of September 4, 2013.

The NASA P-3 aircraft flew the Houston sampling circuit twice on September 4; once in the morning (8-11 AM CST) and once into the early afternoon (11 AM – 2 PM CST). For brevity we focus our analysis on the afternoon circuit; Figure 16 shows that specific flight path indicating 8 different profile spirals. Figure 17 presents time series of altitude and key pollutant concentrations measured during the entire flight. Ozone varies between 20-60 ppb at the surface to about 60 ppb aloft. This inverted ozone pattern is typical in Houston during on-shore flow conditions, where ozone in the shallow boundary layer is much lower than the typical background of 40 ppb. Note that ozone at the surface and aloft converge to about 60-70 ppb later in the day, indicating a well-mixed boundary layer. Total NOy is mostly comprised of nearly equal parts of NO and NO_2, indicating very little aged NOx along the flight paths.

Figure 18 shows simulated ozone on the CAMx 12 km grid at 2 PM September 4 using WRF v3.7/MSKF inputs; the left column shows ozone using the CIG convection module, and the right column shows the difference in ozone with and without the CIG invoked. Five vertical levels are shown: surface, 1.5 km (mid-upper boundary layer), 2.8 km (above boundary layer), 5.4 km (mid-troposphere), and 10.6 km (upper troposphere). Figure 19 shows west-to-east vertical sections of ozone and MSKF cloud water along a single grid row extending from the Big Bend area of the Rio Grande through Houston and the Louisiana Gulf coast, spanning from the surface to 200 mb (~12 km). Figures 20 and 21 show the same set of plots but for NO_2.

Convection impacts CAMx ozone and NO_2 distributions at all levels. Local convection appears as small areas of large concentration differences, whereas regional convection (occurring outside the 12 km grid) is seen mostly aloft as smoother “plumes” of differences coming in through 12 km boundary conditions. Concentration differences can be negative or positive at any level depending on multiple factors: fractional coverage of convective clouds; relative strength of updraft and downdraft profiles in the convective and ambient fractions of each column; and pollutant profile shapes in each column. Generally, convection tends to draw pollutant mass away from low levels and transfer it to mid and upper levels of the troposphere.

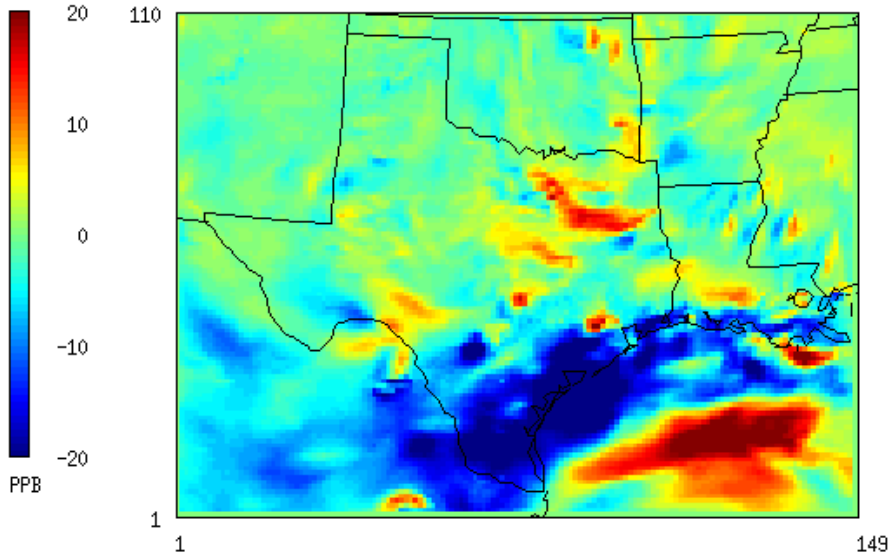

Figure 15. Ozone differences between CAMx/CIG using WRF v3.7/MSKF and WRF v3.6.1/RadKF at 2 PM CST, September 4, 2013. The largest decrement is -49 ppb around the Matagorda/Corpus Christi portion of the Gulf Coast; the largest increment is +29 ppb in the Gulf of Mexico.

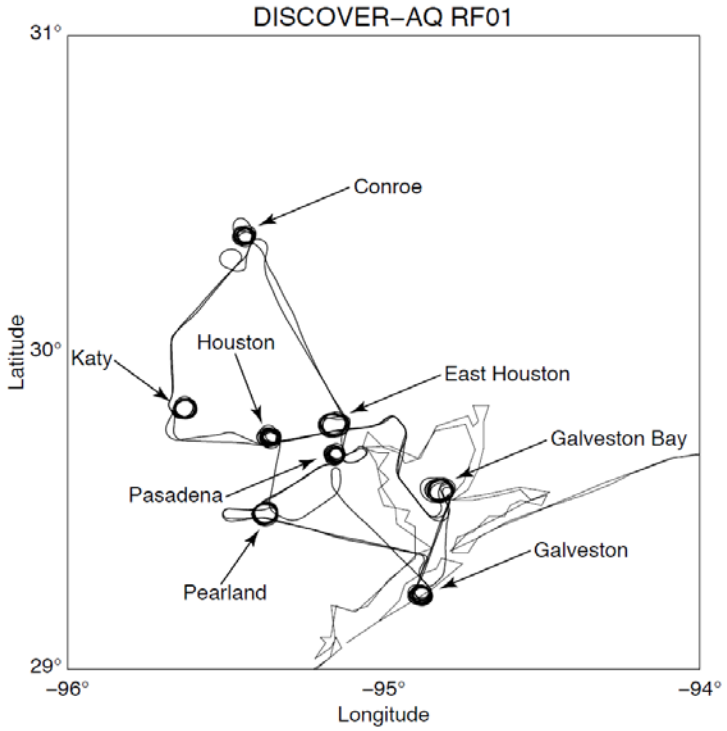

Figure 16. Aircraft flight path 11 AM to 2 PM CST, September 4, 2013 indicating the locations of 8 vertical spirals from which measured profiles were derived.

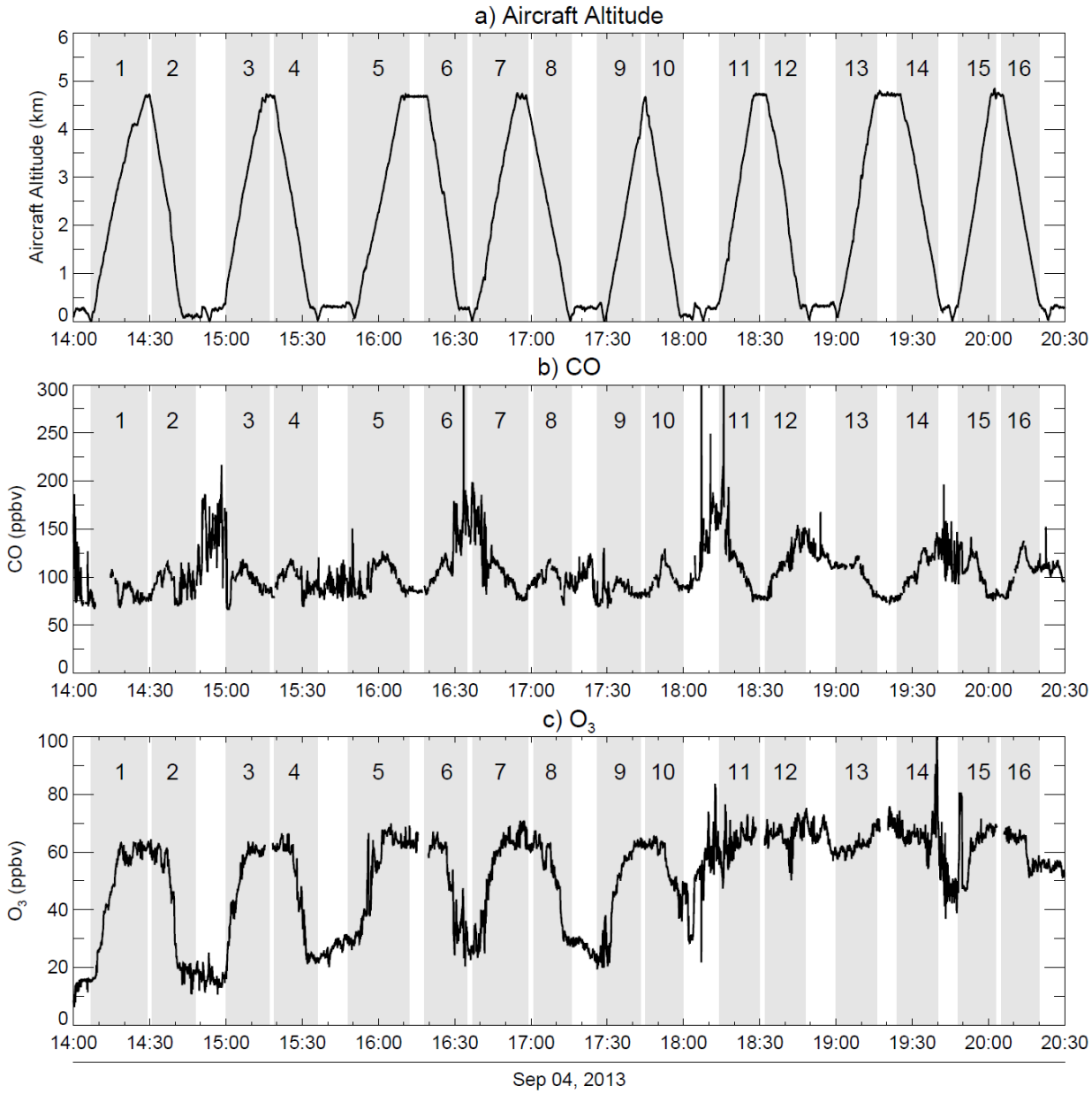

Figure 17. Time series of aircraft altitude and-measured CO, O_3, NO, NO_2, and NOy along the September 4, 2013 DISCOVER-AQ flight track shown in Figure 16.

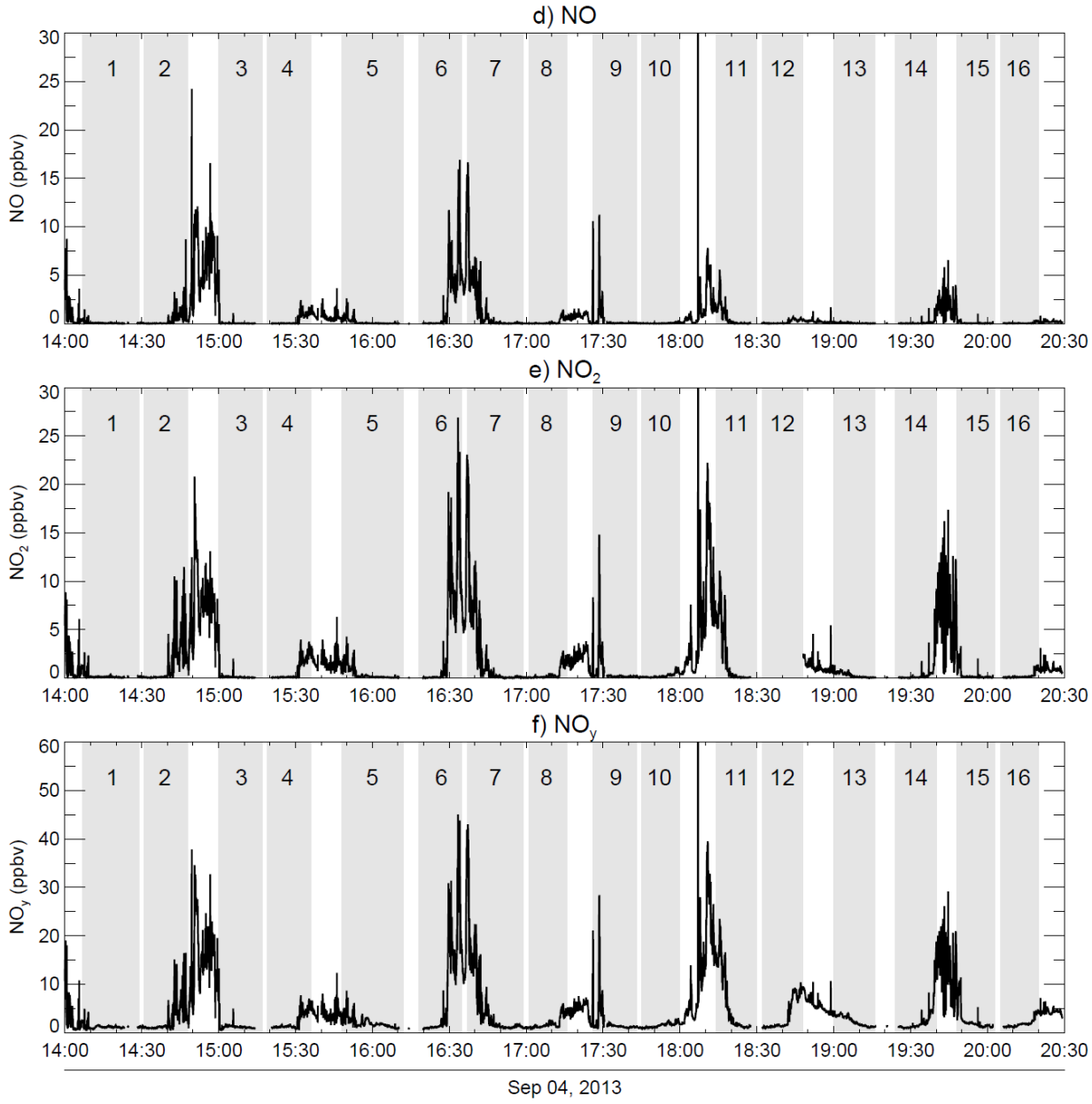

Figure 17 (concluded).

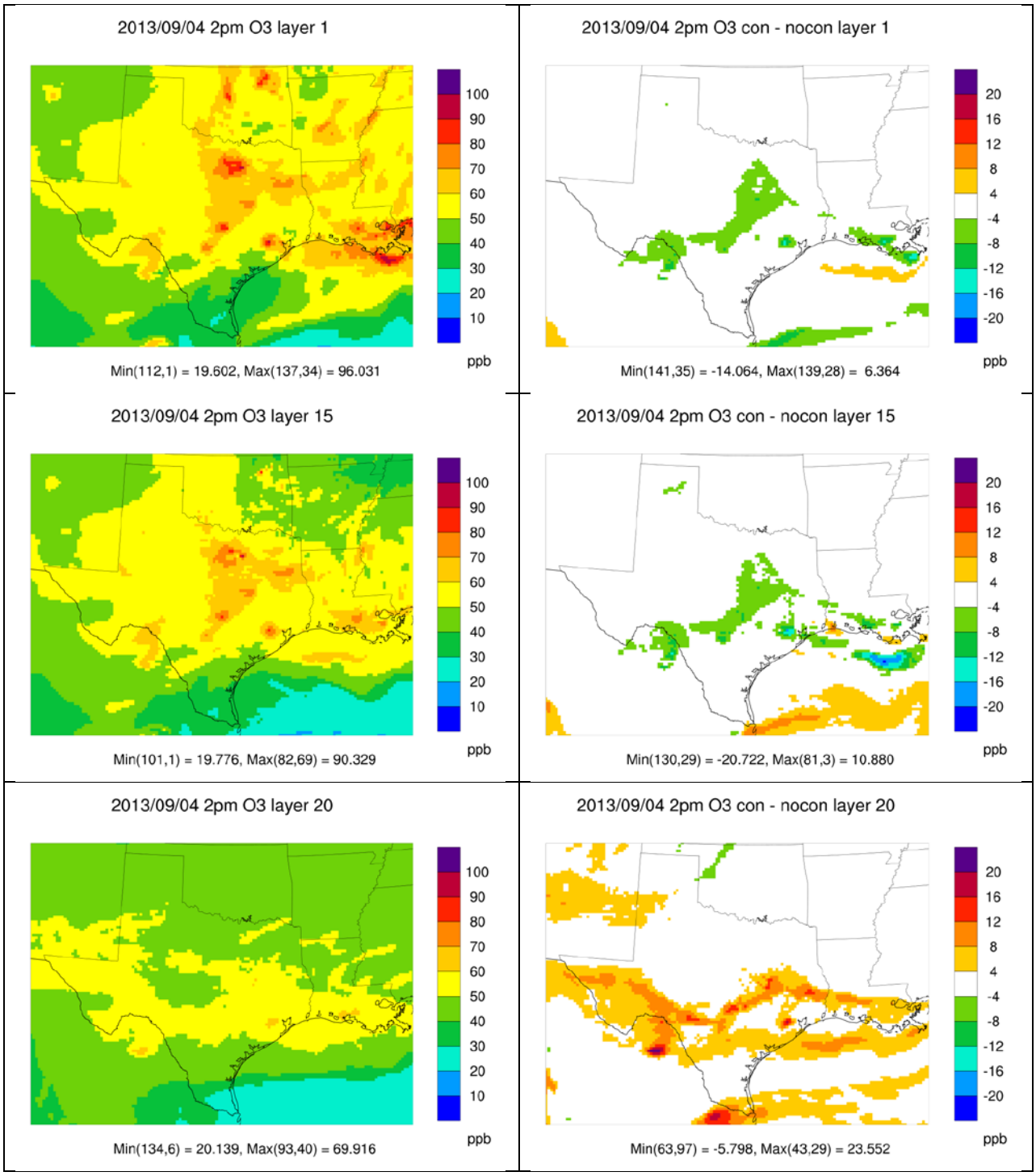

Figure 18. CAMx-simulated ozone on the 12 km modeling grid at 2 PM CST, 4 September, 2013 at five vertical levels (1 = surface, 15 = 1.5 km, 20 = 2.8 km, 24 = 5.4 km, 27 = 10.6 km). Left column shows ozone with CiG convection using WRF v3.7/MSKF fluxes; right column shows ozone differences between CAMx simulations with and without CIG convection. The east-west line in the figure for layer 24 indicates the vertical section in Figures 19 and 21.

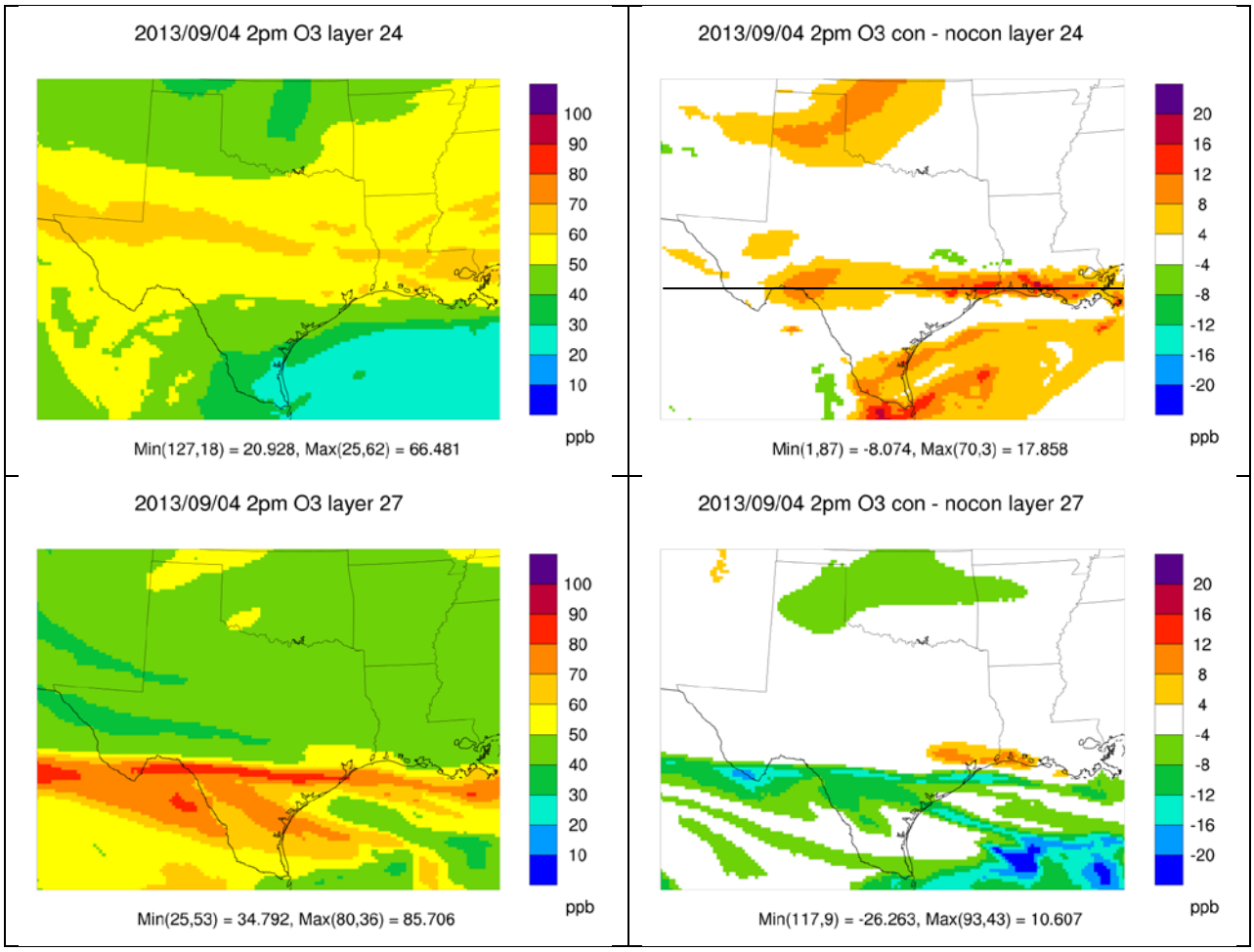

Figure 18 (concluded).

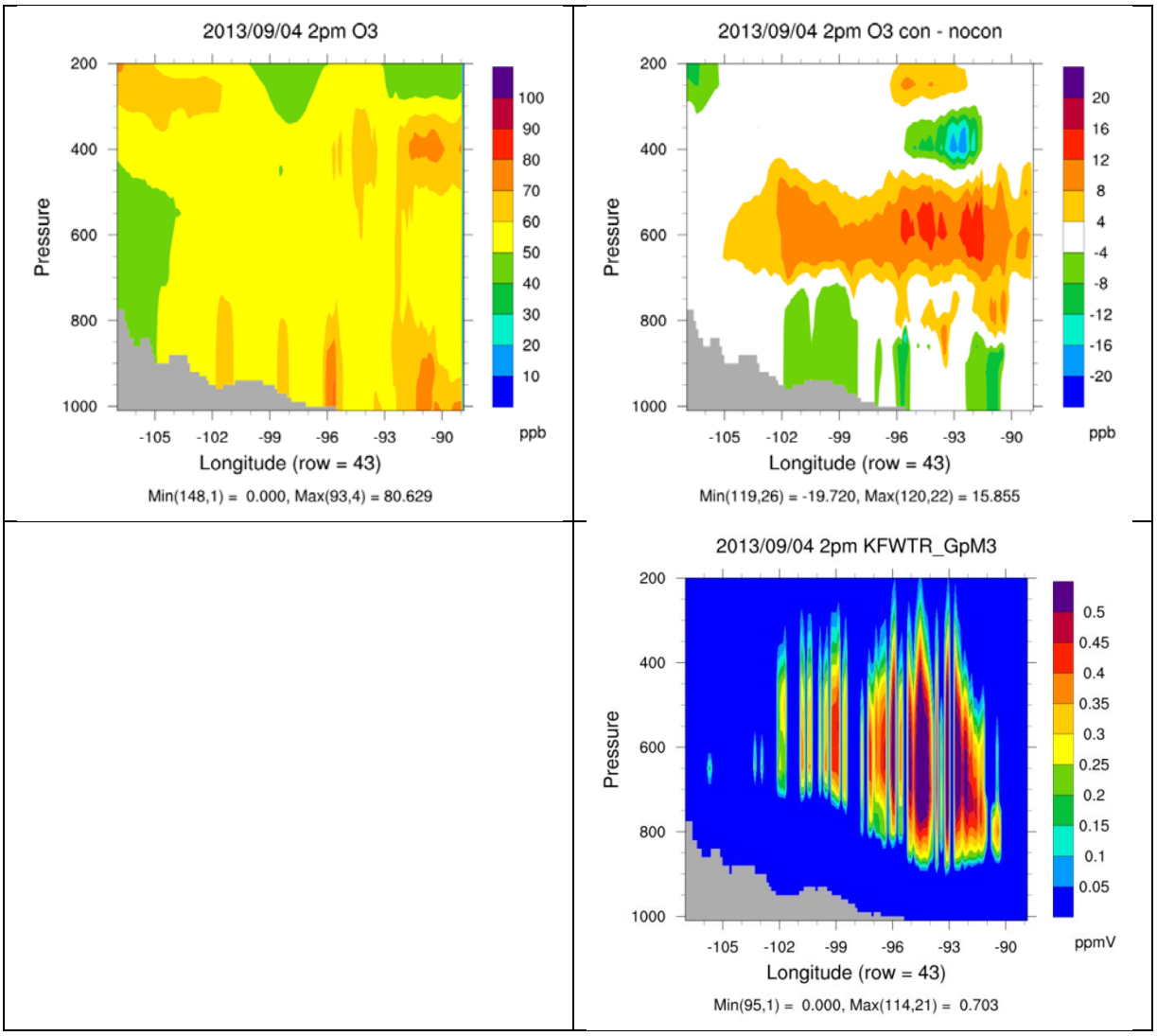

Figure 19. West-east vertical cross section of CAMx-simulated ozone (top) and WRF-simulated MSKF cloud water (bottom) along grid row 43 of the 12 km modeling grid at 2 PM CST, 4 September, 2013. Left column shows ozone with CiG convection using WRF v3.7/MSKF fluxes; right column shows ozone differences between CAMx simulations with and without CIG convection.

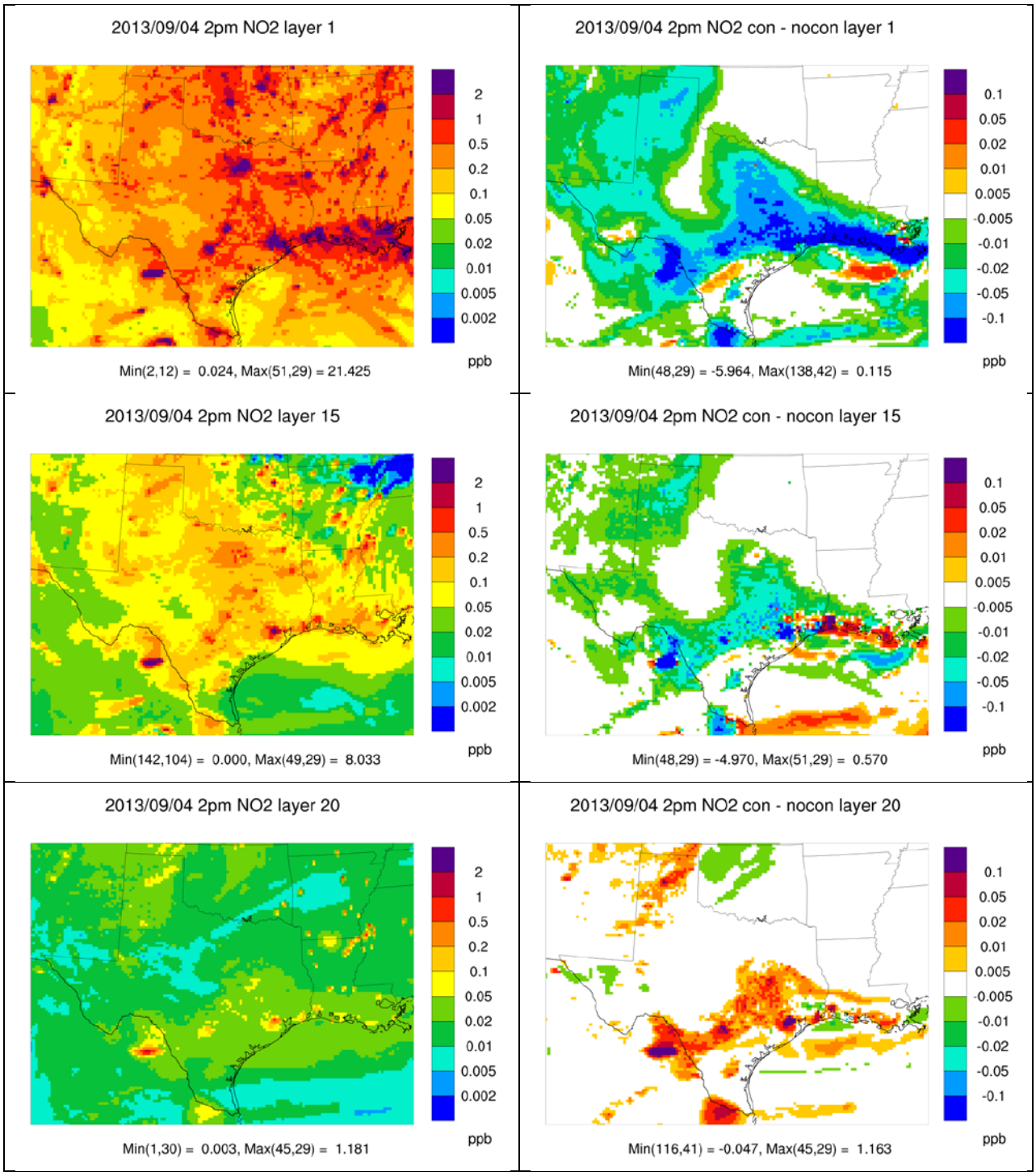

Figure 20. CAMx-simulated NO_2 on the 12 km modeling grid at 2 PM CST, 4 September, 2013 at five vertical levels (1 = surface, 15 = 1.5 km, 20 = 2.8 km, 24 = 5.4 km, 27 = 10.6 km). Left column shows NO_2 with CiG convection using WRF v3.7/MSKF fluxes; right column shows NO_2 differences between CAMx simulations with and without CIG convection. Note that absolute concentrations and differences are plotted on a logarithmic scale.

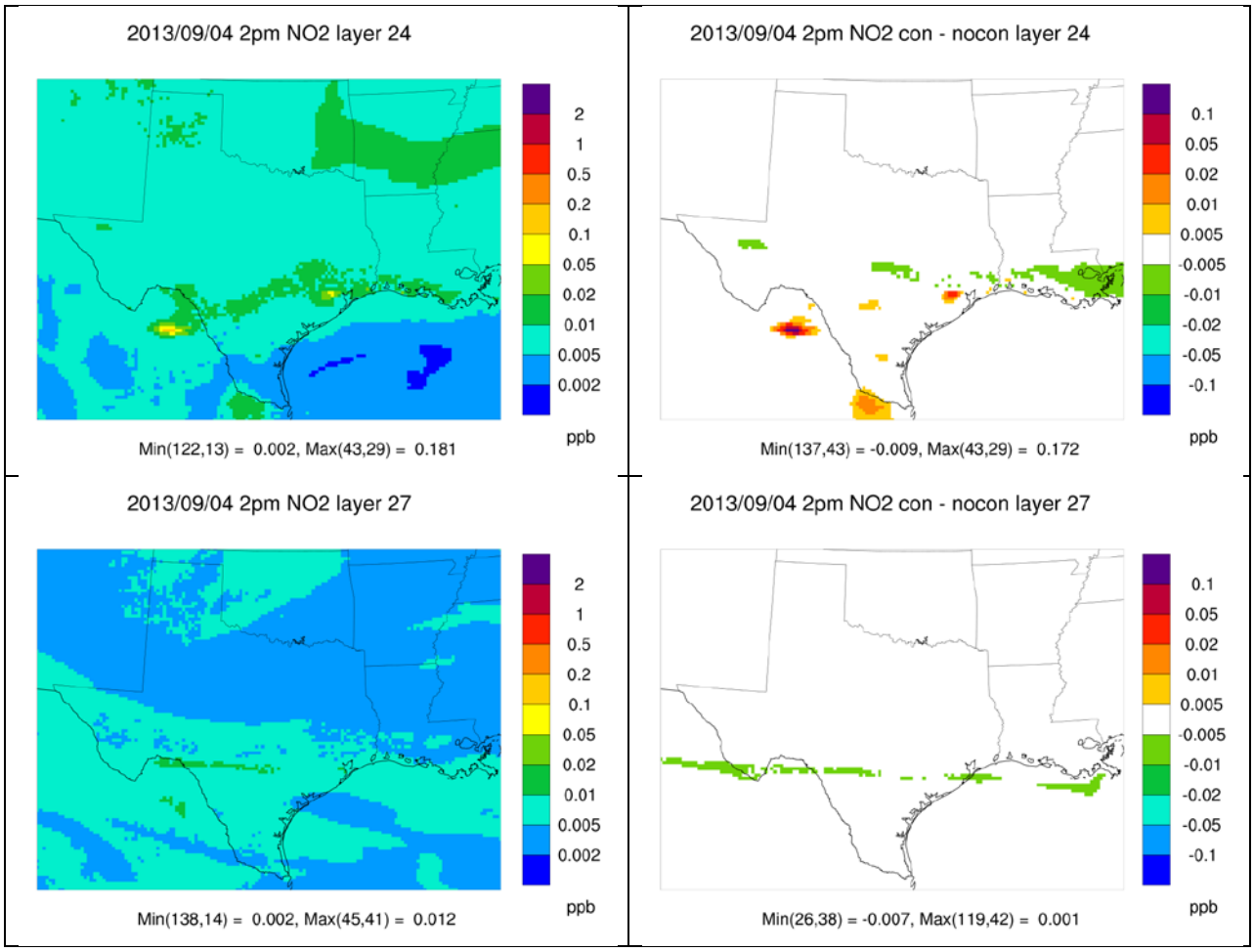

Figure 20 (concluded).

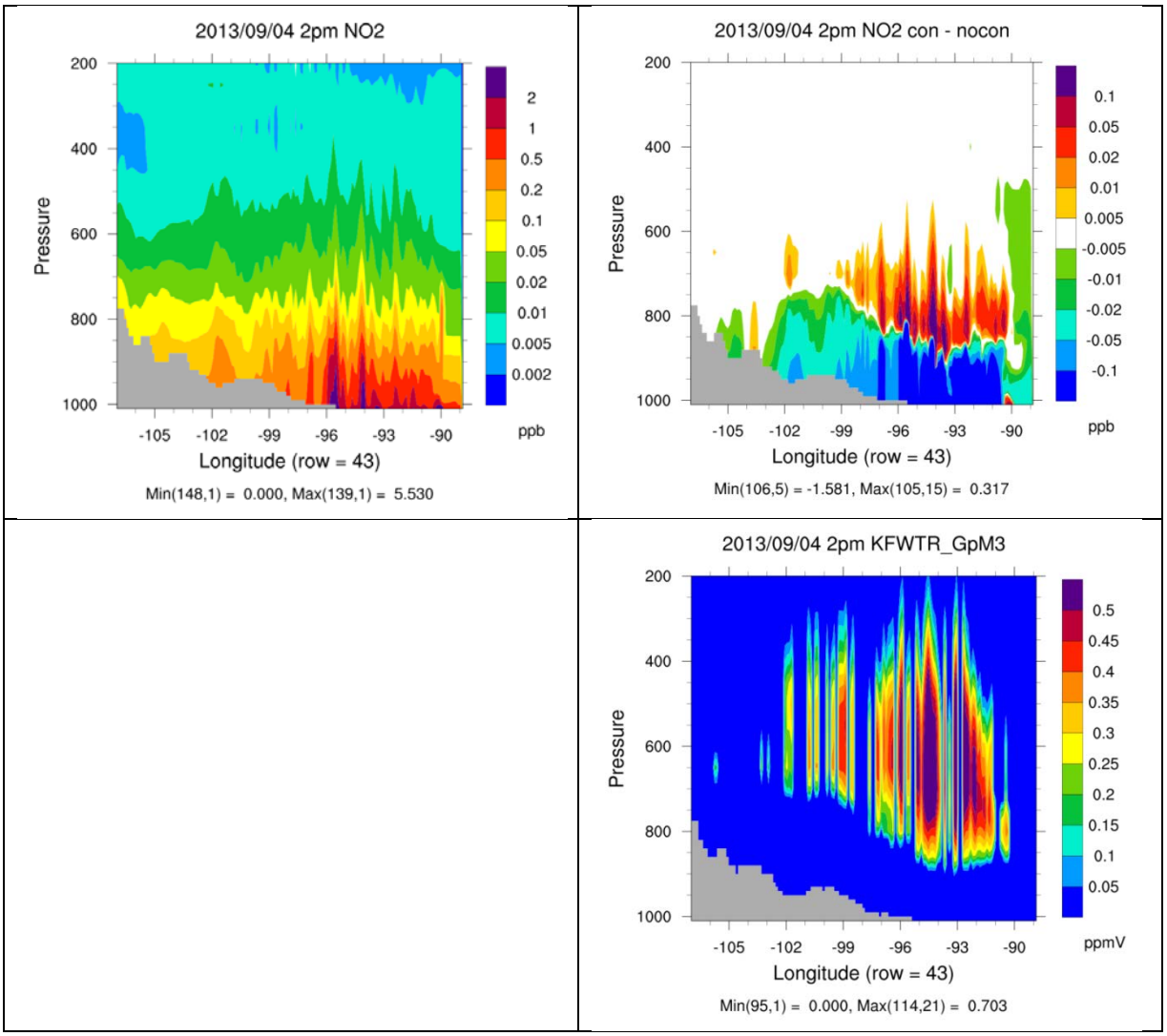

Figure 21. West-east vertical cross section of CAMx-simulated NO_2 (top) and WRF-simulated MSKF cloud water (bottom) along grid row 43 of the 12 km modeling grid at 2 PM CST, 4 September, 2013. Left column shows NO_2 with CiG convection using WRF v3.7/MSKF fluxes; right column shows NO_2 differences between CAMx simulations with and without CIG convection. Note that absolute NO_2 concentrations and differences are plotted on a logarithmic scale.

However, strong downdrafts within the convective fraction, or subsidence within the ambient fraction, can transport higher concentrations aloft downward, as is particularly evident near the top of the model as a net loss.

Figure 22 shows profiles of simulated ozone, total NOy (NOx plus oxidized forms as NOz) and CO paired with measured data for each spiral of the early afternoon flight on September 4, as well as the average among all spirals. Note that NOy is plotted on a logarithmic scale to better illustrate its exponential decrease with altitude, whereas ozone and CO are plotted on a linear scale. Ozone tends to be over predicted along the coastline (Galveston), while slightly under predicted inland. Convection only marginally impacts boundary layer ozone, but results in larger effects aloft that tended to smooth the ozone toward a more uniform profile. Unfortunately these effects occur well above the aircraft profiles so verification is not possible aloft. Both NOy and CO tend to be over predicted in the boundary layer in the non-convective case, but convection improves the agreement with observed profiles by mixing these precursors aloft. Agreement for NOy with CiG convection is particularly good in most cases.

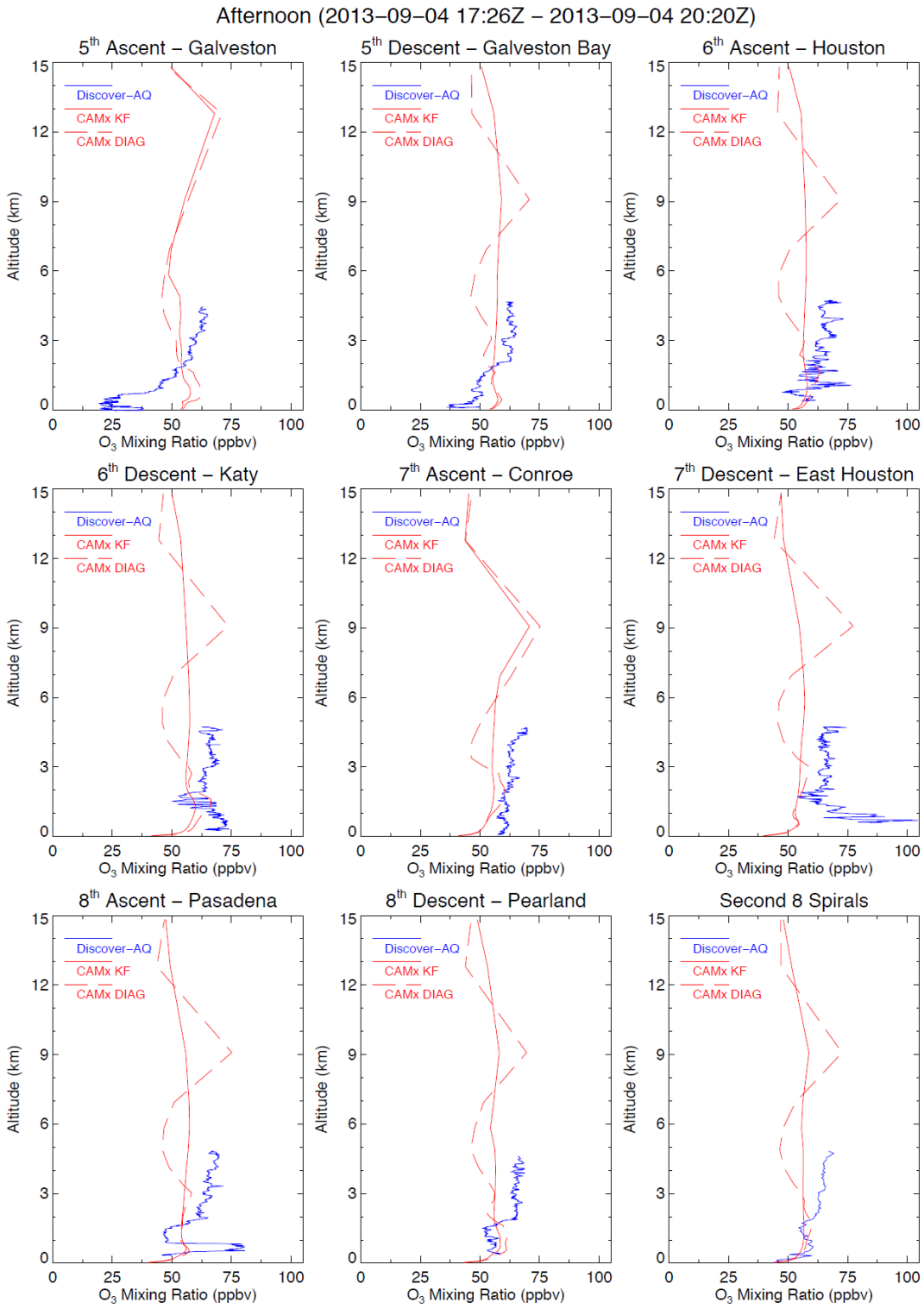

Figure 22(a). Aircraft-measured (blue) and CAMx-simulated profiles of ozone with convection (solid red) and without convection (dashed red) on the afternoon of September 4, 2013.

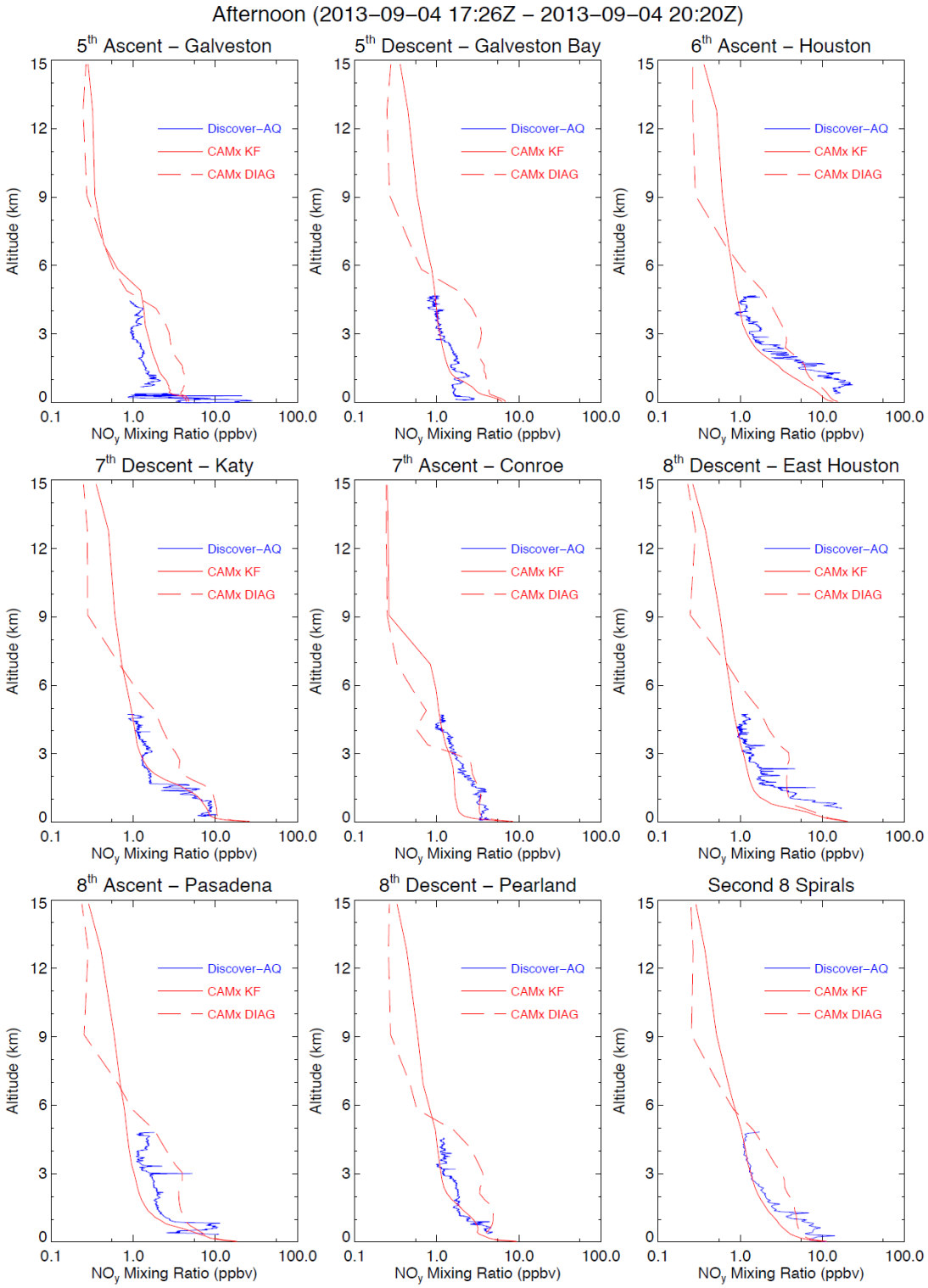

Figure 22(b). As in (a), but for NOy (note logarithmic concentration scale).

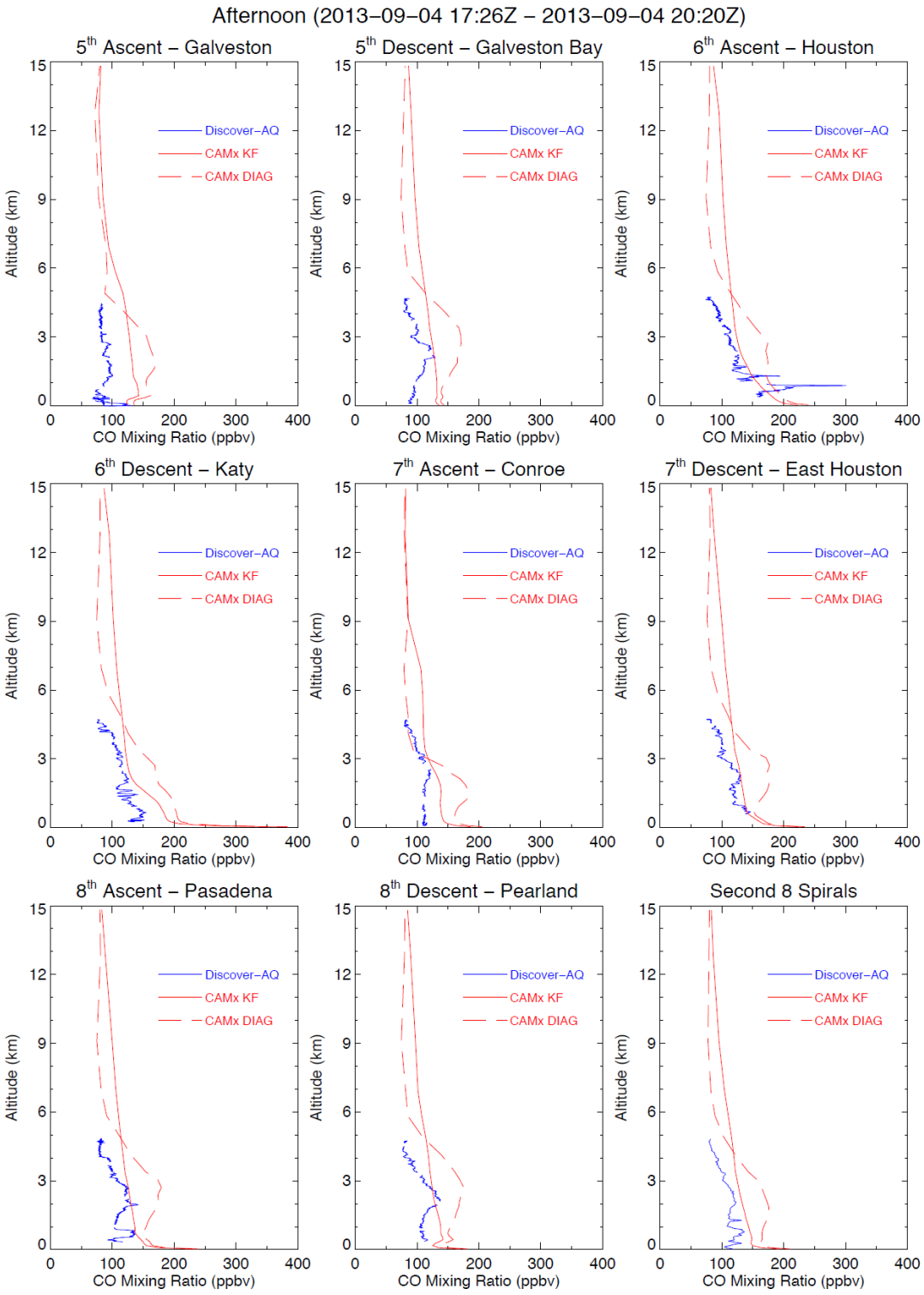

Figure 22(c). As in (a), but for CO.

3.3.2 May 2008

WRF v3.6.1 (with RadKF) was for the May 2008 episode using several configurations of the model in an attempt to identify a sufficiently adequate simulation for testing the CAMx CiG. The best WRF simulation produced organized convection with appropriate structures, according to comparison with radar observations. Convective activity initiated on May 5 in eastern New Mexico, and the thunderstorms that formed there eventually developed into a squall line on May 6. Early on May 6, the location of the squall line in the 12 km grid simulation occurred in Oklahoma rather than North Texas (Figure 23). Later in the day coinciding with the time of the aircraft flight (9 to 12 AM CST), observed convection had moved well east into western Arkansas (Figures 24 and 25), whereas WRF continued to develop weaker and slower-moving convection in central Oklahoma (Figure 26) where a weak surface trough is noted in the weather analysis in Figure 24. Using a combination of simulation results in and around WRF's convective activity allowed us to qualitatively compare the convective mixing model performance with the *in situ* observations.

The NCAR G-V aircraft flight occurred from about 9:30 AM to 12 PM CST on May 6 and sampled tropospheric profiles upwind and downwind of convective activity. Figure 27 shows the specific flight path indicating two ascent segments and two descent segments. Figure 28 presents time series of altitude and key pollutant concentrations measured during the entire flight. Ozone varies from about 50 ppb at the surface to about 150 ppb at 12 km (about the altitude of the tropopause as indicated on Figure 28). Total NOy includes 0-2 ppb contributions from fresh NOx and 1-3 ppb or more from aged forms of nitrogen oxides (NOz). NOz contributes largely to total NOy throughout the atmosphere along the flight path, indicating a dominance of aged nitrogen and long-range transport.

Figure 29 shows simulated ozone on the CAMx 12 km grid at 10 AM May 6 using WRF v3.6.1/RadKF inputs; the left column shows ozone using the CIG convection module, and the right column shows the difference in ozone with and without the CIG invoked. Five vertical levels are shown: surface, 1.4 km (mid-upper boundary layer), 2.7 km (above boundary layer), 5.1 km (mid-troposphere), and 10 km (upper troposphere). Figure 30 shows south-to-north vertical sections of ozone and RadKF cloud water along a single grid column extending from mid-Texas through mid-Oklahoma, spanning from the surface to 200 mb (~12 km). Figures 31 and 32 show the same set of plots but for NO_2.

Convective activity is simulated to be much sparser, weaker and shallower in the area of the START08 flight path relative to observed conditions and relative to the September 2013 episode. CiG impacts to ozone and NO_2 distributions are small and confined mostly to the boundary layer and lower troposphere, with very small effects farther aloft. Very few "plumes" of concentration differences are seen entering the 12 km boundaries, except along the southern boundary in the Gulf of Mexico. This indicates that CiG impacts to these pollutants are confined to rather localized convection within the nested grid. This particular simulation results in much more complex spatial patterns of positive and negative concentration differences in the boundary layer than exhibited in the September 2013 episode.

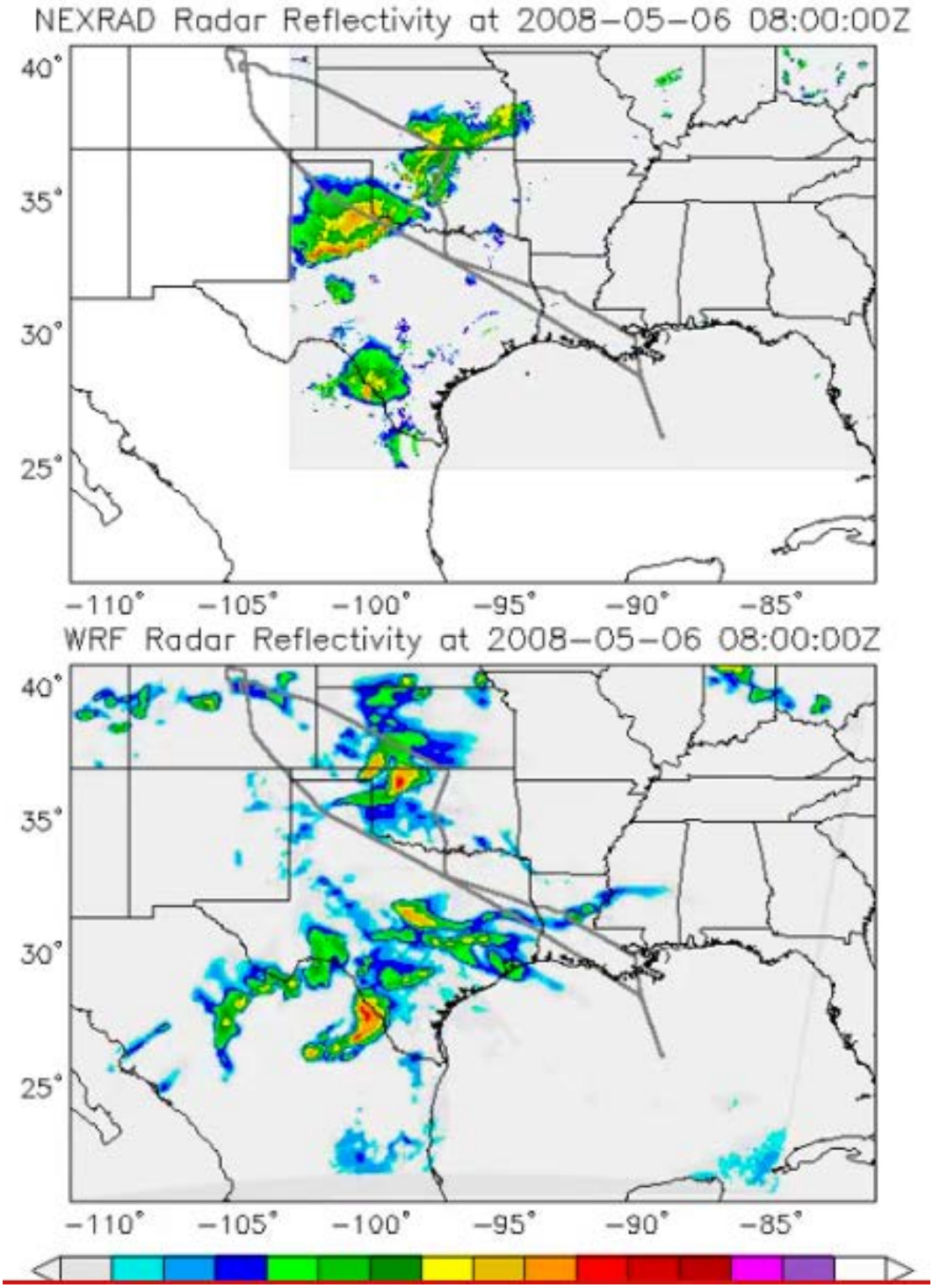

Figure 23. Calculated reflectivity from WRF v3.6.1/RadKF on the 12 km grid at 2 AM CST, May 6, 2008 (bottom) and verifying NEXRAD radar composite (top). The aircraft track is shown in the thick grey line.

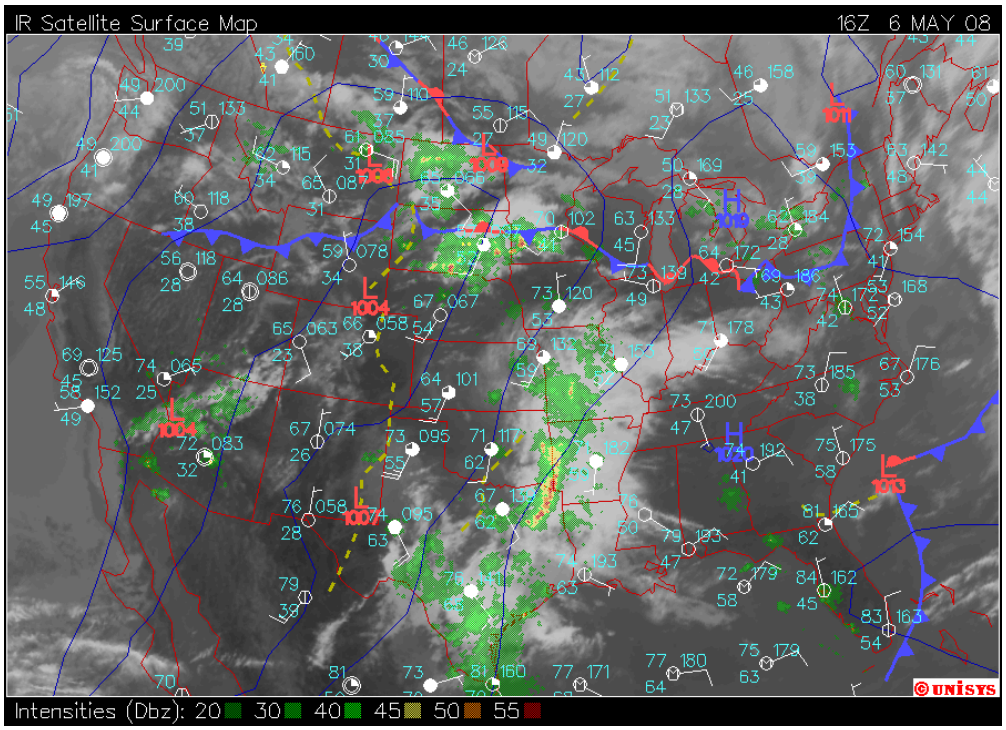

Figure 24. Composite satellite weather chart at 10 AM CST, May 6, 2008.

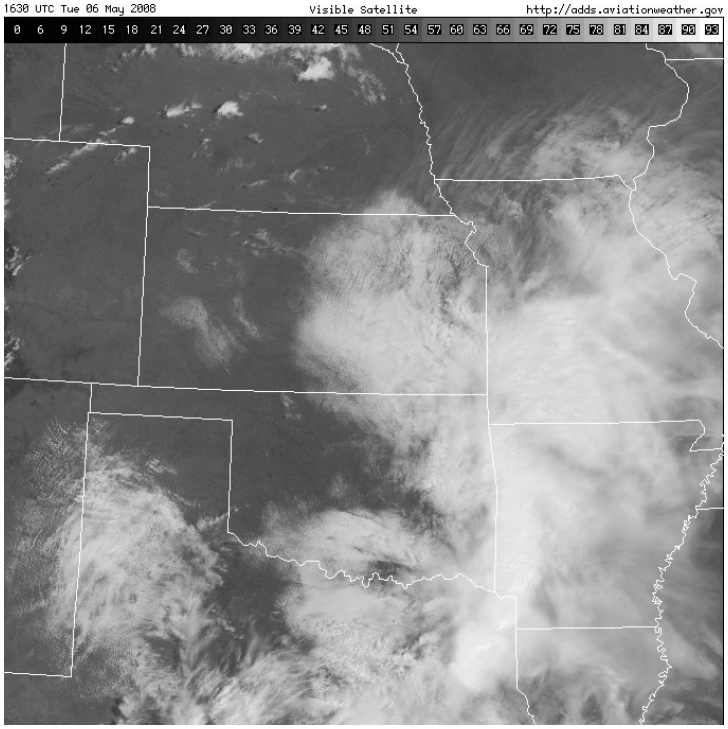

Figure 25. Visible satellite image at 10:30 AM CST, May 6, 2008.

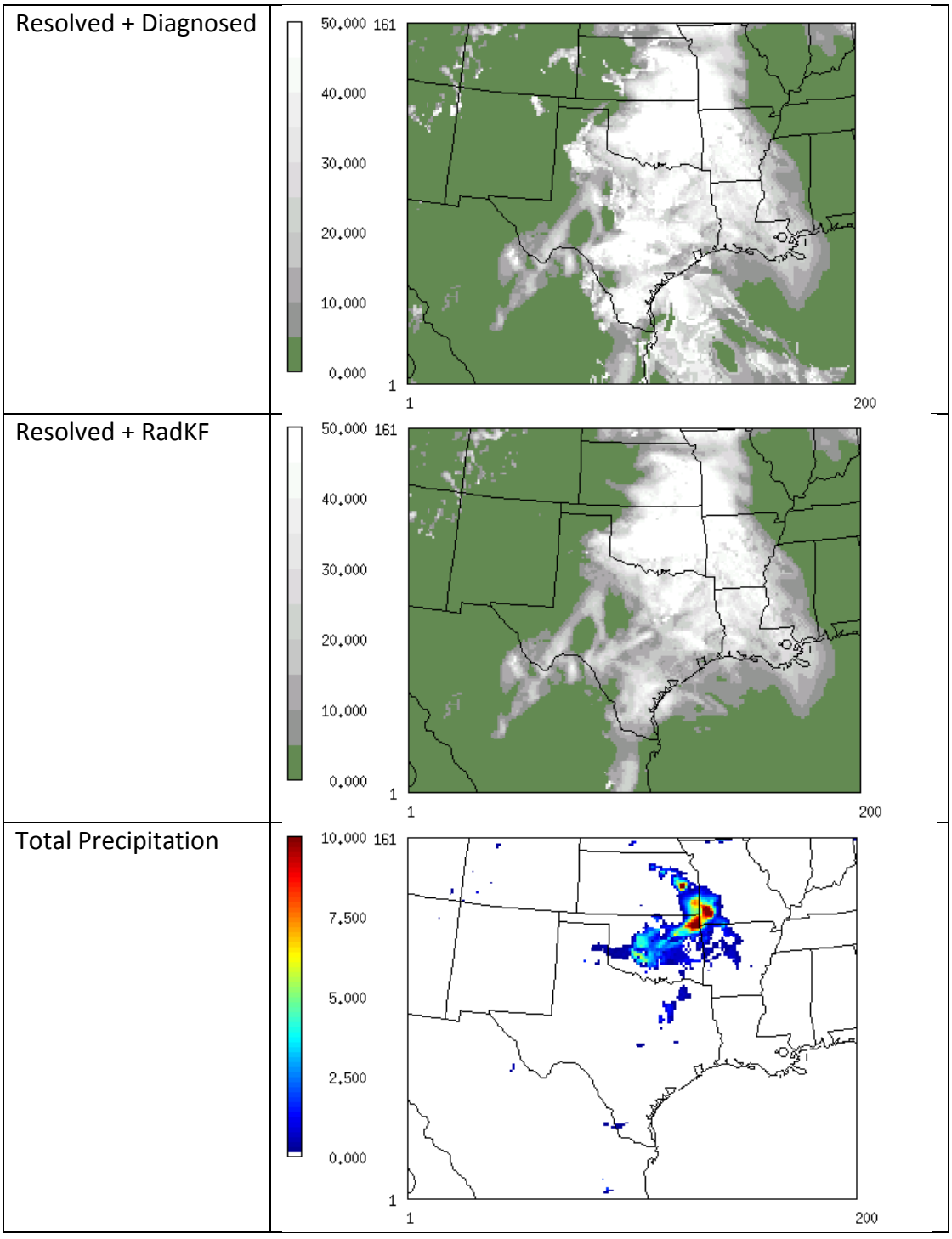

Figure 26. CAMx-ready input total cloud fields (expressed as unitless optical depth) on the 12 km grid for two cases at 10 AM CST, May 6, 2008. (Top) resolved plus diagnosed sub-grid clouds; (middle) resolved plus RadKF sub-grid clouds; (bottom) resolved plus RadKF surface precipitation (mm/hr).

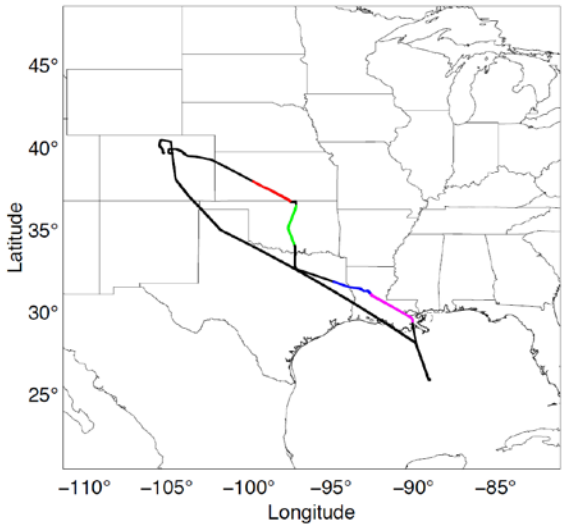

Figure 27. Aircraft flight path 9:30 AM to 12 PM CST, May 6, 2008 indicating location of 4 ascent and descent segments (colored) from which measured profiles were derived.

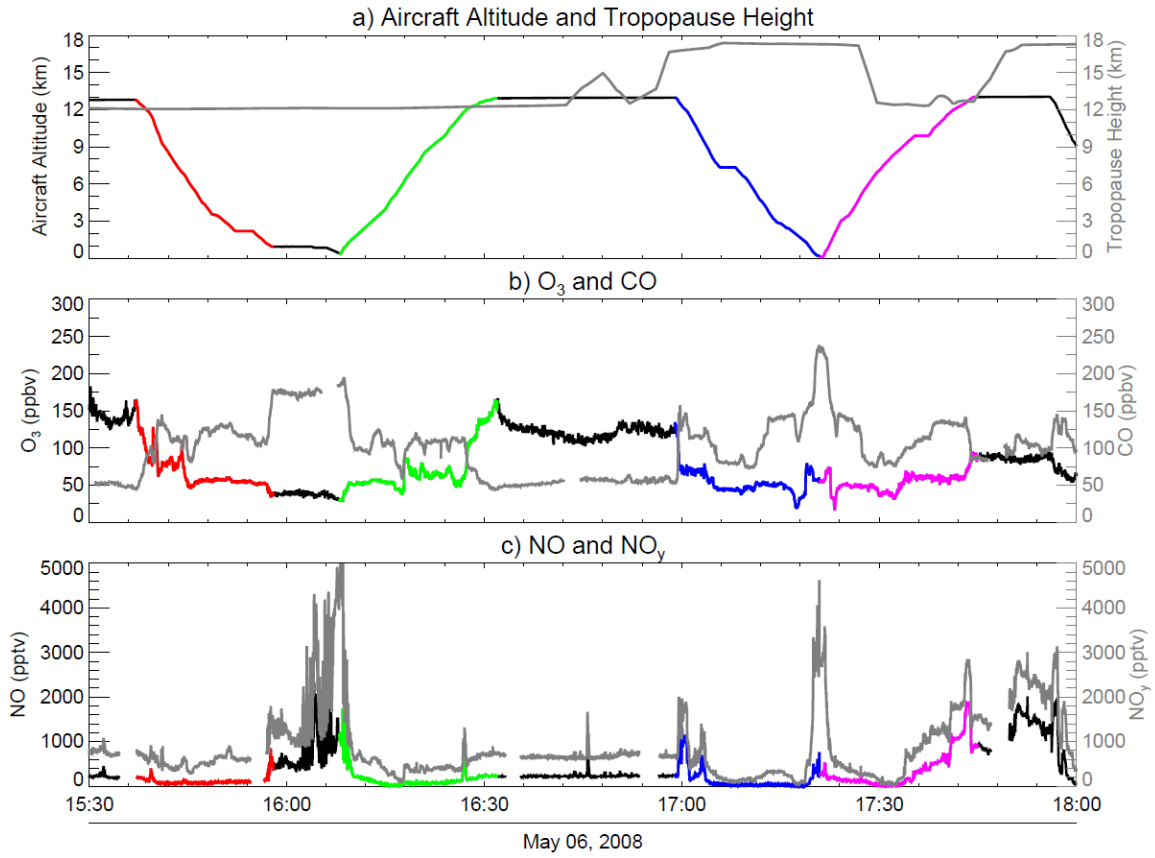

Figure 28. Time series of aircraft altitude and measured CO, O_3, NO, and NOy along the May 6, 2008 START08 flight track shown in Figure 27.

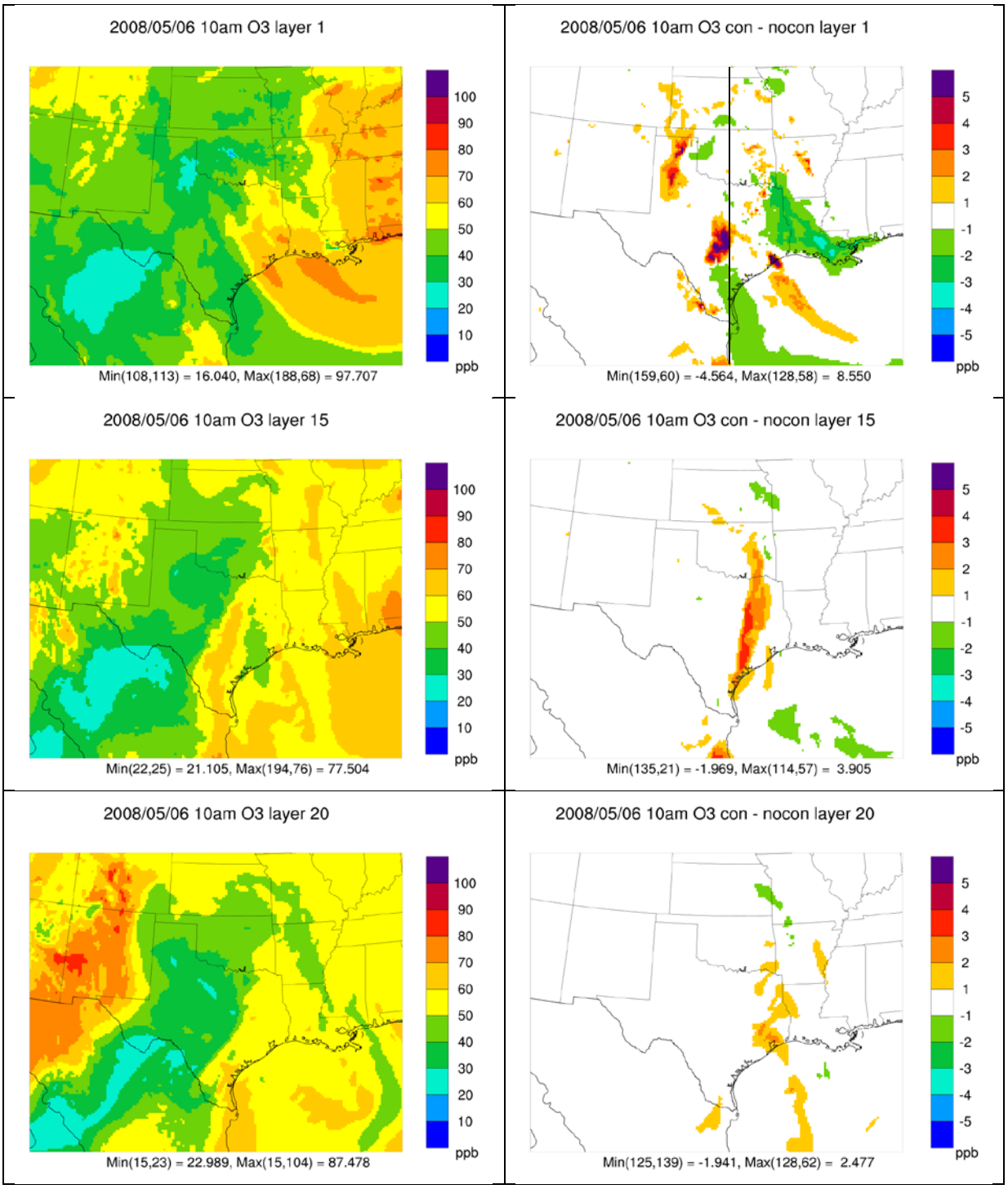

Figure 29. CAMx-simulated ozone on the 12 km modeling grid at 10 AM CST, 6 May, 2008 at five vertical levels (1 = surface, 15 = 1.4 km, 20 = 2.7 km, 24 = 5.1 km, 27 = 10 km). Left column shows ozone with CiG convection using WRF v3.6.1/RadKF fluxes; right column shows ozone differences between CAMx simulations with and without CIG convection. The north-south line in the figure for layer 1 indicates the vertical section in Figures 30 and 32.

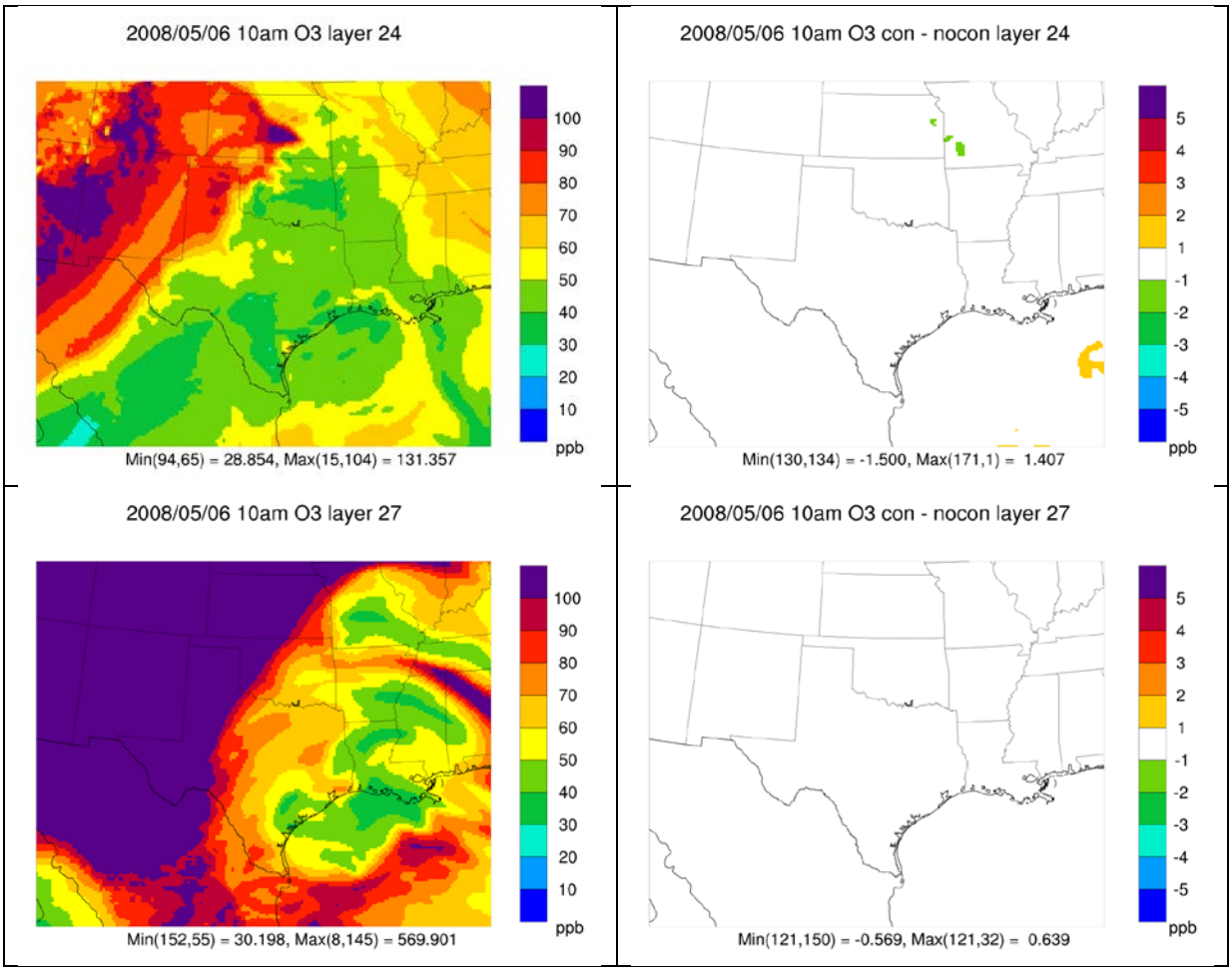

Figure 29 (concluded).

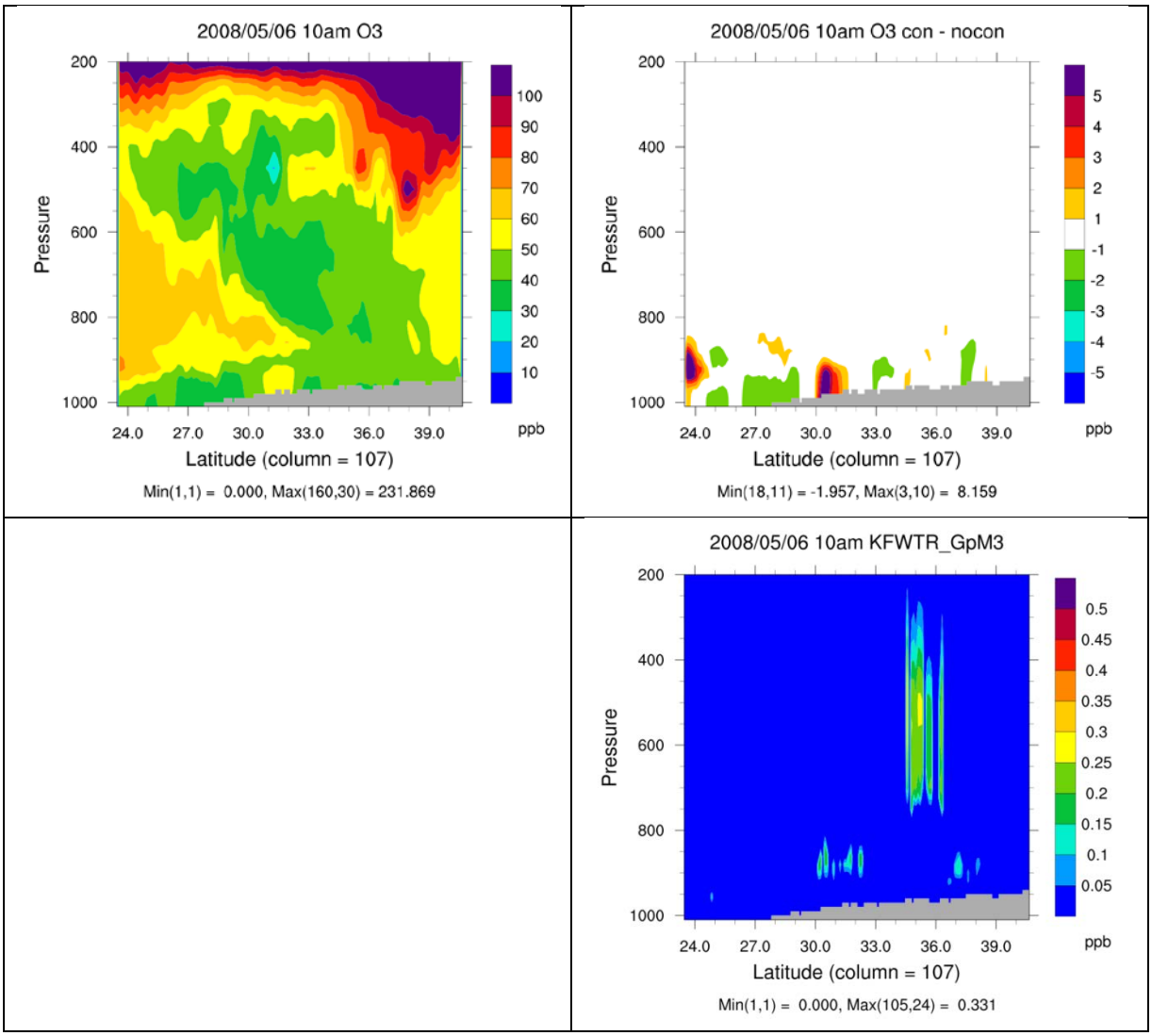

Figure 30. South-north vertical cross section of CAMx-simulated ozone (top) and WRF-simulated RadKF cloud water (bottom) along grid column 107 of the 12 km modeling grid at 10 AM CST, 6 May, 2008. Left column shows ozone with CiG convection using WRF v3.6.1/RadKF fluxes; right column shows ozone differences between CAMx simulations with and without CIG convection.

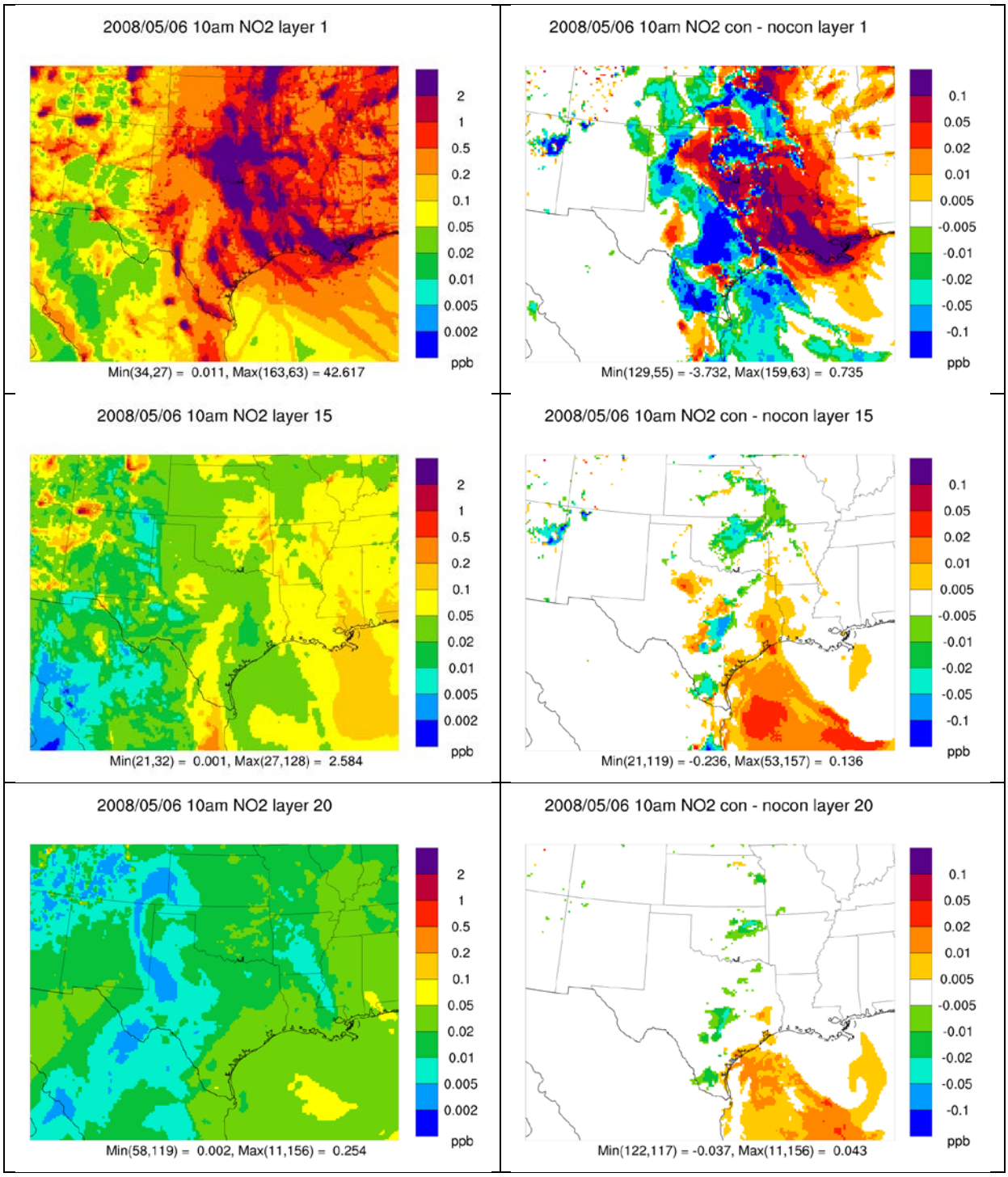

Figure 31. CAMx-simulated NO_2 on the 12 km modeling grid at 10 AM CST, 6 May, 2008 at five vertical levels (1 = surface, 15 = 1.4 km, 20 = 2.7 km, 24 = 5.1 km, 27 = 10 km). Left column shows NO_2 with CiG convection using WRF v3.6.1/RadKF fluxes; right column shows NO_2 differences between CAMx simulations with and without CIG convection. Note that absolute concentrations and differences are plotted on a logarithmic scale.

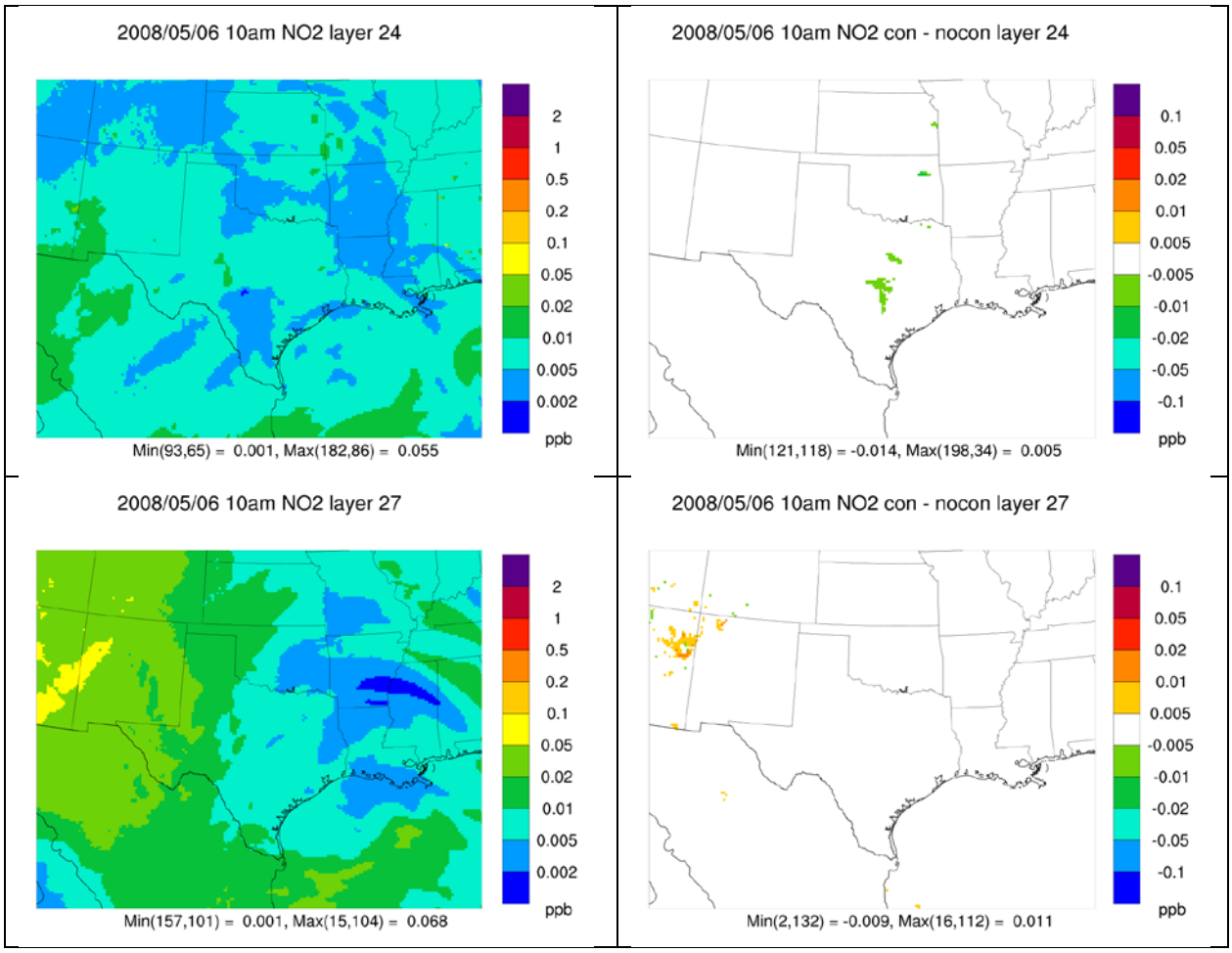

Figure 31 (concluded).

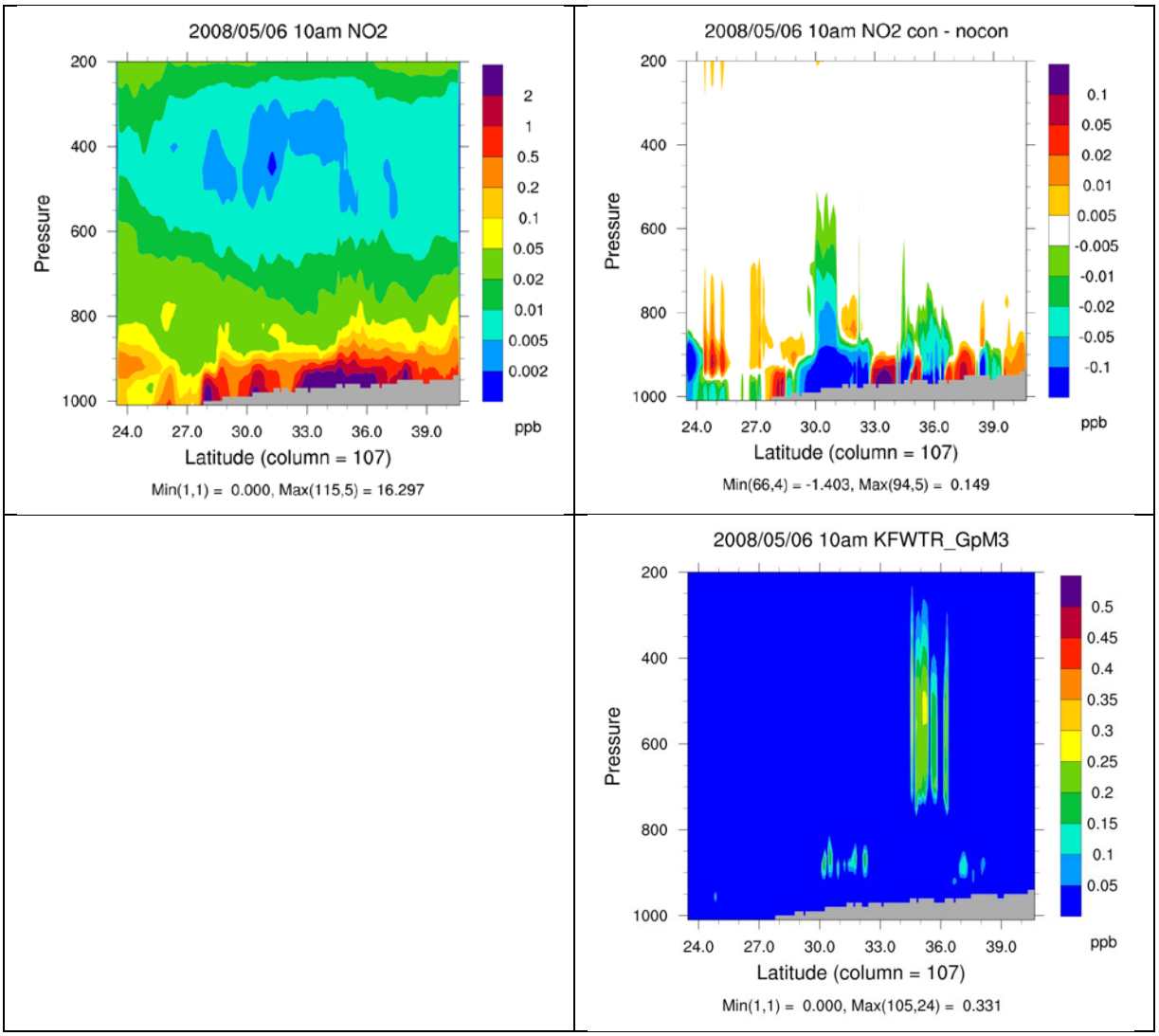

Figure 32. South-north vertical cross section of CAMx-simulated NO_2 (top) and WRF-simulated RadKF cloud water (bottom) along grid column 107 of the 12 km modeling grid at 10 AM CST, 6 May, 2008. Left column shows NO_2 with CiG convection using WRF v3.6.1/RadKF fluxes; right column shows NO_2 differences between CAMx simulations with and without CIG convection. Note that absolute NO_2 concentrations and differences are plotted on a logarithmic scale.

Whereas ozone differences indicate a tendency to mix ozone down into the boundary layer from aloft, NO_2 differences indicate a tendency to ventilate boundary layer NO_2 upwards. This is consistent with the vertical tropospheric gradient of these constituents during this episode (ozone increasing upward, NO_2 decreasing upward) and illustrates that the parameterized convection is a mechanism for bidirectional mixing rather than simply upward transport.

Figure 33 shows profiles of simulated ozone, total NOy (NOx plus oxidized forms as NOz) and CO paired with measured data for each ascent/descent segment of the morning flight on May 6, as well as the average along all four ascent/descent segments. Note again that NOy is plotted on a logarithmic scale, whereas ozone and CO are plotted on a linear scale. The ozone profile throughout the troposphere is much better simulated in the START08 case than in the DISCOVER-AQ case. However, like DISCOVER-AQ, the NOy and CO profiles for START08 tend to be over predicted. CAMx convection contributes imperceptible impacts to ozone and CO at the locations sampled by the aircraft, possibly because of the misplacement and improper intensity/coverage of WRF convection. Convection appears to have impacted NOy more than ozone or CO in these plots, but that is likely a result of the logarithmic scale that enhances small differences. Convection tends to slightly increase NOy over predictions throughout the troposphere. It is possible that these consistent deep increases in NOy are carry-over of aged NOz products (such as nitric acid [HNO_3], peroxyacetyl nitrate [PAN], etc.) from previous days' convection, since activity on May 6 was simulated to be shallow and sparse.

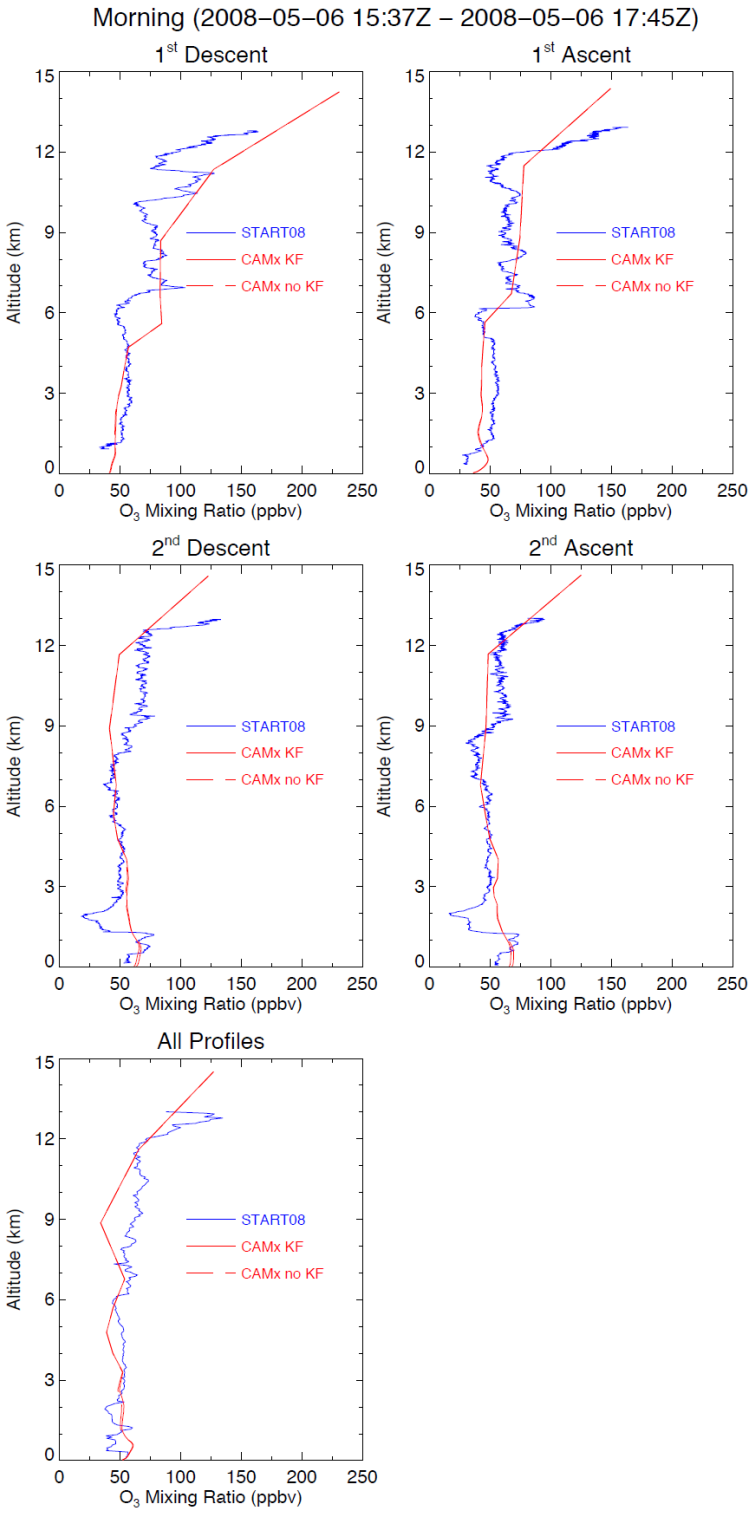

Figure 33(a). Aircraft-measured (blue) and CAMx-simulated profiles of ozone with convection (solid red) and without convection (dashed red) on the morning of May 6, 2008.

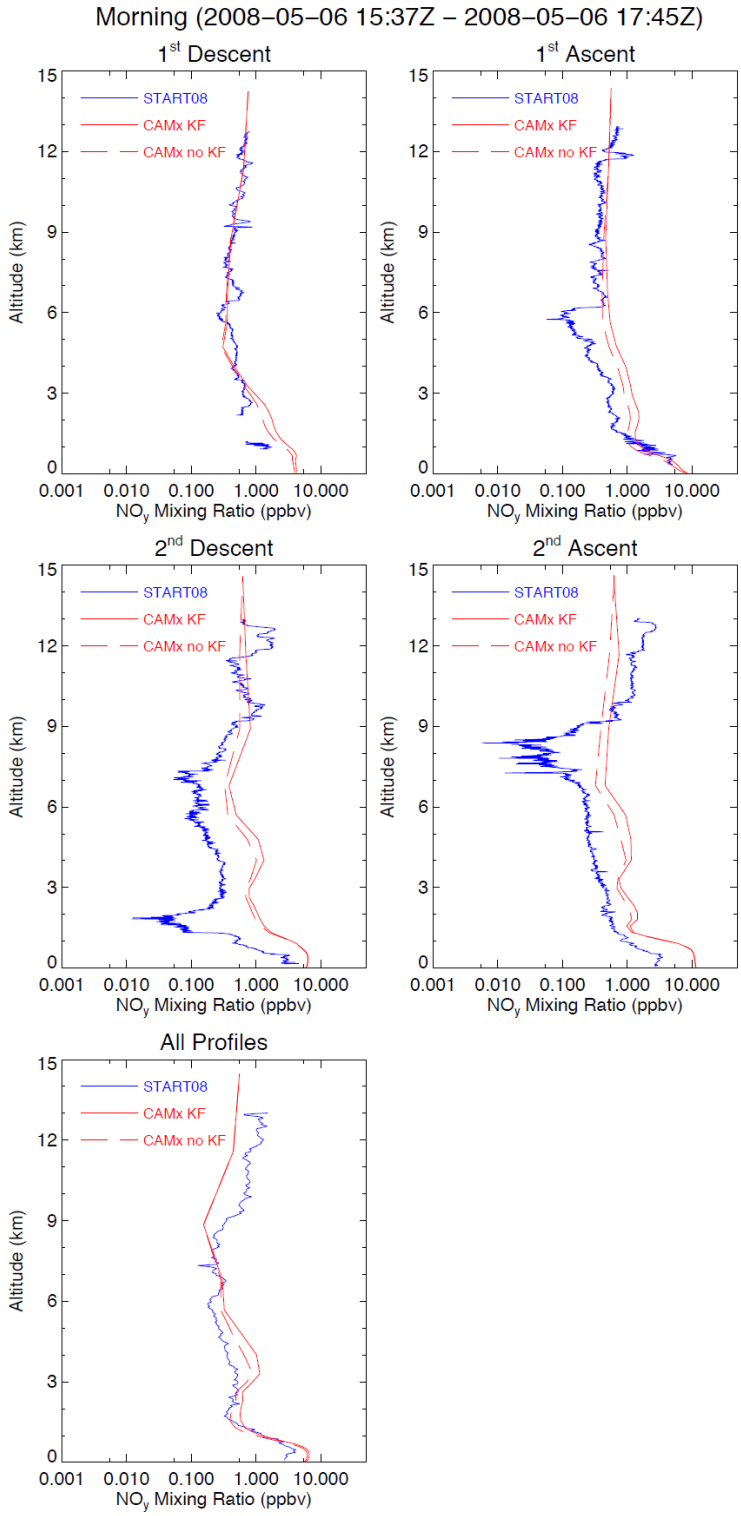

Figure 33(b). As in (a), but for NOy (note logarithmic concentration scale).

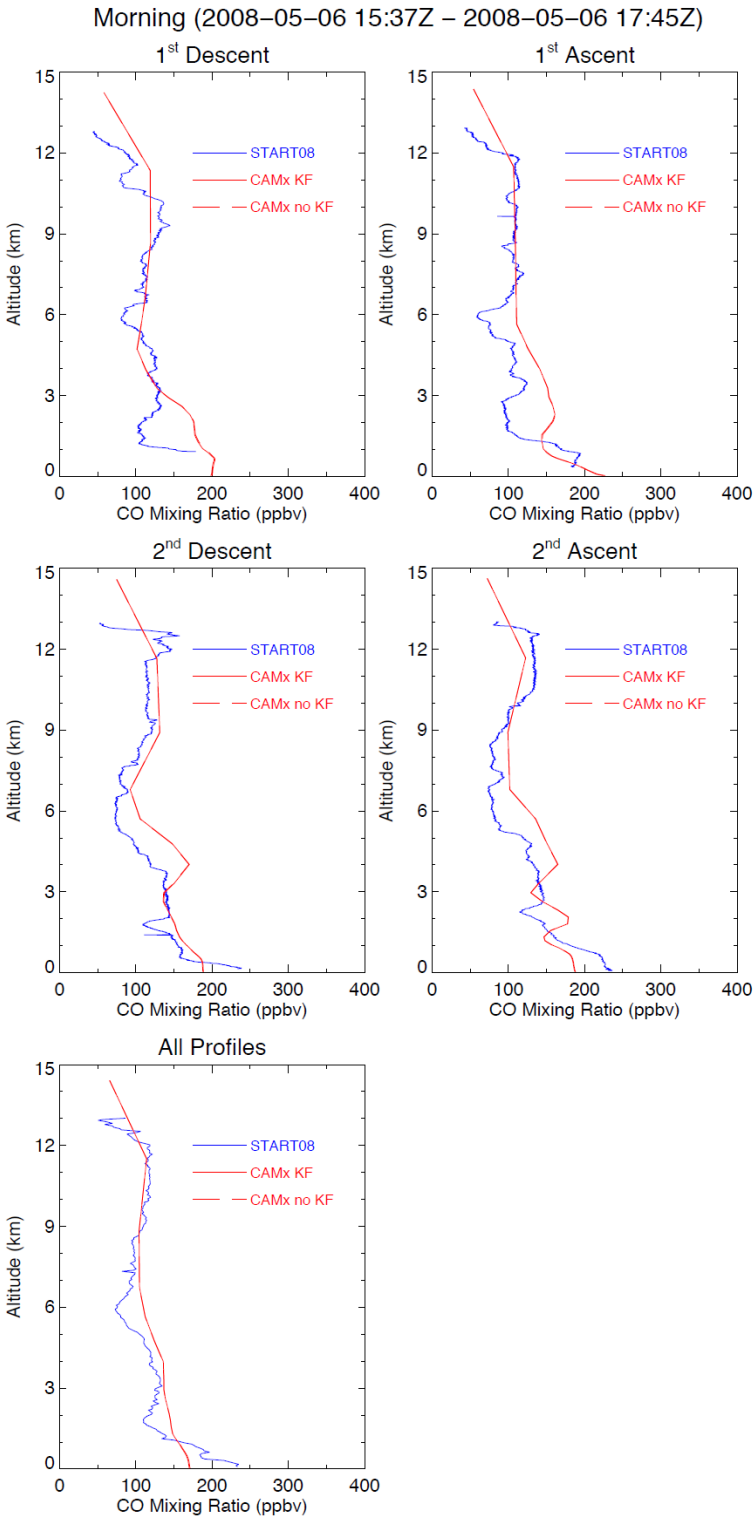

Figure 33(c). As in (a), but for CO.

4.0 AUDITS OF DATA QUALITY

According to requirements for Category III projects, we have conducted audits of data quality at a level that exceeds the minimum 10% of the data generated by the updated software. We followed the approach described in the Quality Assurance Project Plan (QAPP) specifically developed for AQRP Project 14-025. During system development, temporary diagnostic output code was written in the test-bed system to allow for a visual inspection of the evolution of concentrations during transport and chemical processes, and to review all variables used by the modified algorithms and solvers (Section 2). Additional details on the approach to checking correctness of outputs from the new modules are described in Section 4.1. The new CAMx model was run and thoroughly evaluated for two field study campaigns (Section 3). Data generated by CAMx was compared to the output from the original model to ensure that design changes resulted in expected outcomes. CAMx sensitivity results were graphically evaluated to identify and report the impact of the program changes. Concentrations were graphically compared to available measurement data to gauge impacts to model performance. Additional details on the performance evaluation are described in Section 4.2.

4.1 Quality Assurance During Development

Code development was directed by the project manager and co-principal investigator, Mr. Christopher Emery. Mr. Emery was assisted by Mr. Jeremiah Johnson as needed to develop and test specific process modules. Mr. Emery oversaw construction of all facets of new code, ensured seamless integration among new subroutines and within the CAMx program flow, and led all testing and quality assurance steps.

Basic process testing and debugging was performed by first running the CiG framework inside a standalone test-bed driver program, in which simple user-controlled cloud environments were provided to the CiG to ensure proper operation and data passing between the cloud column and ambient column. Functionality, interfacing, performance and design constraints for the new module were evaluated. Good FORTRAN coding practices and FORTRAN compile-time checks helped to confirm that the PiG subroutines were coded properly. 100% of input and output data from these test-bed runs were analyzed as part of the QA evaluation. Section 2.2.1 documents results from these activities.

Upon successful initial testing, the CiG framework was implemented as a CAMx sub-model, and tied into the model's MPI and OMP parallelization. WRFCAMx and CAMx were tested by running short (2 day) test cases using input data streams from the updated WRFCAMx system. This testing focused on identifying implementation bugs and performance issues. Alternative approaches were considered and tested to minimize speed impacts. Roughly 50% of the data from the 2-day tests were analyzed as part of the QA evaluation. Sections 2.2.2 and 2.2.3 document results from these activities.

4.2 CAMx System Evaluation

The CAMx system evaluation was conducted by applying the updated model for two existing modeling datasets covering the September 2013 DISCOVER-AQ and May 2008 START08 field campaigns. The testing methodology and results are described in Section 3.

Models and datasets accessed for this study consisted of the following:

1) WRF v3.6.1 and v3.7 from NCAR (http://www2.mmm.ucar.edu/wrf/users/download/get_source.html);
2) CAMx modeling system data for September 2013 (Kemball-Cook et al., 2014b; Johnson et al., 2013, 2015);
3) CAMx modeling system data for 2008 (Emery et al., 2013; McDonald-Buller et al., 2013);
4) Measurement data from the DISCOVER-AQ (Pickering, 2013) and START08 field campaigns (Pan et al., 2010).

The WRF model versions used in this project have been evaluated and vetted by NCAR prior to their public release via the WRF download portal shown above.

Emery et al. (2013) fully evaluated the 2008 CAMx modeling database in a past AQRP project. The modeling system tended to over-predict ozone in the south-central US (including Texas) throughout the year, with the largest over predictions occurring during the warm season (June-August). Emery et al. (2013) attributed the ozone over predictions to chemistry issues (as opposed to transport issues) and the tendency to predict very high ozone over the Gulf, which was then brought inland.

Johnson et al. (2013, 2015) and Kemball Cook et al. (2014b) developed the 2013 CAMx modeling database for TCEQ and evaluated performance against measurement data throughout Texas and the Gulf Coast. The model typically over-predicted ozone throughout Texas, and incremental changes to the modeling configuration were able to ameliorate some of the performance issues.

Validation and quality assurance procedures have been independently conducted on DISCOVER-AQ measurement datasets by the respective reporting institutions to flag missing or suspect data due to a variety of causes. Only final quality-assured un-flagged data were used in the comparisons to modeling data. Further information on the DISCOVER-AQ data management plan is provided by NASA (2011).

Following the completion of the START08 field program in 2008, the project data sets were quality controlled by the instrument scientists, the project principal investigators, and the data support staff of the Earth Observation Laboratory (EOL) of the National Center for Atmospheric Research (NCAR) (Pan et al., 2010). Data are archived in the NCAR EOL online data repository (http://data.eol.ucar.edu/master_list/?project=START08). Only final quality-assured un-flagged data were used in the comparisons to model simulations.

Modeling results from the modified version of CAMx for the September 2013 episode were compared to CAMx runs using the original (unmodified) program to evaluate changes in the resulting output fields and model speed. All job scripts and standard output and error files were reviewed to ensure that the model tests were constructed and applied properly, and that the model ran correctly.

The project team then conducted a detailed evaluation of CAMx results against *in situ* aircraft measurements from the START08 and DISCOVER-AQ databases. Staff at both Ramboll Environ and TAMU developed new graphical products with which to facilitate the evaluation. The team collaborated on evaluating these products and identifying any clear problems in the modeling results. Solutions were developed to improve certain details within the CAMx CiG framework or to fix bugs or performance issues not caught during the code development and testing tasks. Additional model runs were performed and evaluated as necessary. Particular focus was placed on how well CAMx captures or evolves features in the profiles of NOx, ozone and other key tracers during monitored convective periods, and how the WRF/CAMx modeling system performed overall in characterizing convection and its impacts to spatial and temporal pollutant distributions.

5.0 CONCLUSION AND RECOMMENDATIONS

A new sub-grid convective cloud module has been incorporated into the CAMx photochemical grid model. The new "Cloud-in-Grid" (CiG) treatment includes a new vertical convective transport component for both in-cloud and ambient fractions of the grid column, as well as explicit aqueous chemistry and wet scavenging within the sub-grid cloud compartment. The CAMx/CiG is linked to updates to the WRF meteorological model's Kain-Fritsch sub-grid cumulus scheme developed by EPA/NERL, which now passes specific sub-grid cloud flux and other information directly to CAMx. The new algorithm has been thoroughly quality assured, and process testing in serial and OMP/MPI-parallel modes indicates no substantial impact to overall model speed. The CiG offers two advantages over approaches employed in other off-line photochemical grid models: (1) a direct and consistent link between WRF and CAMx models that removes the need to independently re-diagnose convection location, depth, intensity, and water contents; and (2) the inclusion of both in-cloud convective fluxes and compensating vertical motions in the ambient portion of the cell.

CAMx/CiG was evaluated by applying the model to multi-day episodes in 2008 and 2013 when ozone and precursor concentration measurements were available from aircraft measurement campaigns during START08 and DISCOVER-AQ, respectively. Specific days during each episode were selected for the presence of various convective modes. In both episodes, substantial effort was expended to identify an adequate configuration of WRF that resulted in useable simulations of observed convective patterns and intensity. Whereas a relatively good simulation of convective activity was achieved for September 4, 2013 around Houston, Texas using the WRF/MSKF scheme, only a marginally acceptable simulation of convection was achieved for May 6, 2008 across Oklahoma and northern Texas using the WRF/RadKF scheme. The project schedule precluded us from attempting WRF/MSKF simulations for START08. As a result, the project focused on examining the behavior of the convective mixing parameterization in locations of model-simulated convection during the two cases. The consequences of convective mixing on the horizontal and vertical distribution of key gas-phase constituents (ozone, NOy and CO) were qualitatively assessed for plausibility and were compared to aircraft observations in nearby locations and similar times.

In the September 2013 simulation, convection impacted ozone and NO_2 distributions at all levels throughout the troposphere as a result of local convection in southeast Texas, as well as contributions from convection throughout the region. Complex patterns of positive and negative impacts resulted from multiple factors, including the amount of cloud fractional coverage, relative strength of updraft and downdraft profiles, and pollutant profile shapes in each column. Generally, convection tended to draw pollutant mass away from low levels and transfer it to mid and upper levels of the troposphere. In some areas, however, strong downward motion was particularly evident, especially near the top of the model where concentrations decreased in areas of convective activity.

Analysis of simulated and aircraft-measured pollutant profiles from DISCOVER-AQ indicated plausible model responses to local convection, even if the simulated profiles were not well

replicated in the baseline (no convection) case. As expected, convection tended to smooth ozone toward a more uniform profile. Both NOy and CO tended to be over predicted in the boundary layer in the non-convective case, but convection improved the agreement with observed profiles by mixing these precursors aloft. Agreement for NOy in the convection case was particularly good for most profiles and for the average over all profiles, indicating a better representation of ozone precursor emissions.

In the May 2008 simulation, convective activity was simulated to be much sparser, weaker and shallower relative to observed conditions and relative to the September 2013 episode. The tropospheric ozone profile was better simulated in this case, while the NOy and CO profiles tended to be over predicted. CiG impacts to ozone and NO_2 distributions were small and confined mostly to the boundary layer and lower troposphere, with very small effects farther aloft. This resulted in much more complex spatial patterns of positive and negative concentration differences in the boundary layer than exhibited in the September 2013 episode. Whereas convection indicated a tendency to mix ozone down into the boundary layer from aloft, it tended to ventilate boundary layer NOx upwards. All simulated convective activity was locally isolated in the Oklahoma area on the May 6 START08 flight day, so little effects from regional convection were immediately obvious across the modeling domain. However, a small yet consistent increase in NOy throughout the troposphere may have been the result of a carry-over of aged NOz products (HNO_3, PAN, etc.) from previous days' convection, since it could not be explained by the sparse/shallow activity on May 6.

We have confirmed that the convective mixing parameterization produces substantial changes in constituent mixing ratio in areas of model-simulated convection, with smaller yet potentially widespread contributions from regional convection. The lack of impact at aircraft-sampled locations in May 2008 is a consequence of insufficient model-simulated convection rather than any deficiency in the convective mixing parameterization.

An important assumption in this CIG implementation is that a grid cell contains two well-mixed air volumes: in-cloud air and ambient air. The two-volume approach is equivalent to a three-volume approach treating in-cloud updraft air, in-cloud downdraft air, and ambient air with highly-efficient mixing among the two in-cloud parcels. A three-volume CiG could be developed with in-cloud interactions controlled by a mixing coefficient. Such an implementation would require additional internal memory and computing time, and it is not clear how to parameterize and tune the in-cloud mixing coefficient. Tuning would require several well-modeled convective cases with corresponding observations, none of which are available during DISCOVER-AQ or START-08. It is not possible to determine from the model-observation comparisons above whether the two-volume assumption is appropriate.

Based on the project results summarized above, we recommend follow-on projects that address additional evaluation and necessary extensions to other areas of the model:

- Test and evaluate CiG impacts to PM; evaluate PM aqueous chemical production, wet scavenging and surface accumulation, and long-range transport;

- Test and evaluate CiG in conjunction with explicit top boundary condition inputs now available in CAMx v6.20 from either GEOS-Chem or MOZART global chemistry models, as well as with the additional of aircraft emissions at cruise altitude and lightning NOx;
- Extend CiG to operate with CAMx probing tools (source apportionment, decoupled direct method, process analysis, and reactive tracers), perform testing and evaluate impacts.

6.0 REFERENCES

Alapaty, K., J.A. Herwehe, T.L. Otte, C.G., Nolte, O.R. Bullock, M.S. Mallard, J.S. Kain, J. Dudhia, 2012. Introducing subgrid-scale cloud feedbacks to radiation for regional meteorological and climate modeling. *Geophys. Res. Lett.*, 39, L24809, doi:10.1029/2012GL054031.

Alapaty, K., O.R. Bullock, J.A. Herwehe, R. Gilliam, C.G. Nolte, T. Otte, J. Kain, J. Dudhia, 2013. The Kain-Fritsch Scheme: Science Updates and revisiting gray-scale issues from the NWP and regional climate perspectives. Presented at the 2013 WRF workshop. http://cfpub.epa.gov/si/si_public_record_report.cfm?dirEntryId=258289.

Alapaty, K., J.S. Kain, J.A. Herwehe, O.R. Bullock, M.S. Mallard, T.L. Spero, C.G. Nolte, 2014. Multiscale Kain-Fritsch scheme: formulations and tests. Presented at the 13th Annual Community Modeling and Analysis System (CMAS) Conference, Chapel Hill, NC, October 27-29, 2014.

Belikov, D.A., et al., 2013. Off-line algorithm for calculation of vertical tracer transport in the troposphere due to deep convection. *Atmos. Chem. Phys.*, 13, 1093-1114, doi:10.5194/acp-13-1093-2013.

EPA, 2014. Modeling Guidance for Demonstrating Attainment of Air Quality Goals for Ozone, PM2.5 and Regional Haze. US Environmental Protection Agency, Research Triangle Park, NC. Draft, December 2014. http://www.epa.gov/ttn/scram/guidance/guide/Draft-O3-PM-RH-Modeling_Guidance-2014.pdf.

Emery, C., J. Jung, J Johnson, G. Yarwood, S. Madronich, G. Grell, 2010. Improving the Characterization of Clouds and Their Impact on Photolysis Rates Within the CAMx Photochemical Grid Model, Final Report: Work Order 582-7-84005-FY10-23. Prepared for the Texas Commission on Environmental Quality, Austin, TX, by ENVIRON International Corporation, Novato, CA (August).

Emery, C., B. Koo, T. Sakulyanontvittaya, G. Yarwood, 2013a. Improving CAMx GREASD PiG Efficiency, Final Report: Work Order 582-11-10365-FY13-09. Prepared for the Texas Commission on Environmental Quality, Austin, TX, by ENVIRON International Corporation, Novato, CA (August).

Emery, C., E. Tai, G. Yarwood, M. Lin, 2013b. Using Global and Regional Models to Represent Background Ozone Entering Texas, Final Report: AQRP Project 12-011. Prepared for the Texas Air Quality Research Program, University of Texas at Austin, and the Texas Commission on Environmental Quality, Austin, TX, by ENVIRON International Corporation, Novato, CA, and Princeton University/NOAA Geophysical Fluid Dynamics Laboratory, Princeton, NY (November).

ENVIRON, 2014. User's Guide: Comprehensive Air quality Model with extensions, v6.10. Prepared by ENVIRON International Corporation, May 2014 (www.camx.com).

Foley, K.M., Roselle, S.J., Appel, K.W., Bhave, P.V., Pleim, J.E., Otte, T.L., Mathur, R., Sarwar, G., Young, J.O., Gilliam, R.C., Nolte, C.G., Kelly, J.T., Gilliland, A.B., Bash, J.O., 2010. Incremental testing of the Community Multiscale Air Quality (CMAQ) modeling system version 4.7, *Geosci. Model Dev.*, 3, 205-226, doi:10.5194/gmd-3-205-2010, 2010.

Herwehe, J.A., K. Alapaty, T.L. Spero, C.G. Nolte, 2014a. Increasing the credibility of regional climate simulations by introducing subgrid-scale cloud-radiation interactions. *J. Geophys. Res.*, 119, 5317-5330, doi:10.1002/2014JD021504.

Herwehe, J.A., K. Alapaty, O.R. Bullock, 2014b. Evaluation of Developments Toward a Multiscale Kain-Fritsch Convection Parameterization in WRF. Poster presented at the 13th Annual Community Modeling and Analysis System (CMAS) Conference, Chapel Hill, NC, October 27-29, 2014.

Johnson, J., E. Tai, P. Karamchandani, G. Wilson, G. Yarwood, 2013. TCEQ Ozone Forecasting System, Final Report: Work Order 582-11-10365-FY13-13. Prepared for the Texas Commission on Environmental Quality, Austin, TX; by ENVIRON International Corporation, Novato, CA (November).

Johnson, J., G. Wilson, D.J. Rasmussen, G. Yarwood, 2015. Daily Near Real-Time Ozone Modeling for Texas, Final Report: Work Order 582-11-10365-FY14-16. Prepared for the Texas Commission on Environmental Quality, Austin, TX; by ENVIRON International Corporation, Novato, CA (January).

Kain, J.S., 2004. The Kain-Fritsch convective parameterization: An update. *J. Appl. Meteor.*, 43, 170–181.

Kemball-Cook, S., J. Johnson, G. Yarwood, 2012. Evaluating TCEQ NOx Emission Inventories Using Satellite NO2 Data, Final Report: Work Order 582-11-10365-FY12-08. Prepared for the Texas Commission on Environmental Quality, Austin, TX; by ENVIRON International Corporation, Novato, CA (August).

Kemball-Cook, S., J. Johnson, G. Yarwood, 2013. Continuation on Use of Satellite Nitrogen Dioxide (NO2) Data, Final Report: Work Order 582-11-10365-FY13-10. Prepared for the Texas Commission on Environmental Quality, Austin, TX; by ENVIRON International Corporation, Novato, CA (August).

Kemball-Cook, S., C. Emery, E. Tai, J. Jung, J. Johnson, G. Yarwood, 2014a. Improved Stratosphere-to-Troposphere Transport and Evaluation of Upper Tropospheric Winds in CAMx, Final Report: Work Order 582-11-10365-FY14-15. Prepared for the Texas Commission on Environmental Quality, Austin, TX; by ENVIRON International Corporation, Novato, CA (August).

Kemball-Cook, S., T. Pavlovic, J. Johnson, L. Parker, D.J. Rasmussen, J. Zagunis, L. Ma, G. Yarwood, 2014b. Analysis of Wildfire Impacts on High Ozone Days in Houston, Beaumont, and Dallas-Fort Worth in 2012 and 2013. Final Report: Work Order 582-11-10365-FY14-19. Prepared for the Texas Commission on Environmental Quality, Austin, TX; by ENVIRON International Corporation, Novato, CA (July).

McDonald-Buller, E., Y. Kimura, C. Wiedinmyer, C. Emery, E. Tai, 2013. The Effects of Uncertainties in Fire Emissions Estimates on Predictions of Texas Air Quality, Final Report: AQRP Project 12-018. Prepared for the Texas Air Quality Research Program, University of Texas at Austin, and the Texas Commission on Environmental Quality, Austin, TX, by the University of Texas at Austin, the National Center for Atmospheric Research, Boulder, CO, and ENVIRON International Corporation, Novato, CA (November).

NASA, 2011. Earth Venture 1: Data Management Plan. Prepared by the National Aeronautics and Space Administration, DISCOVER-AQ Science Directorate, Langley Research Center (D-AQ-DMP-01, Version 1, 6/22/2011).

Pan, L.L., K.P. Bowman, E.L. Atlas, S.C. Wofsy, F. Zhang, J.F. Bresch, B.A. Ridley, J.V. Pittman, C.R. Homeyer, P. Romashkin, W.A. Cooper, 2010. The Stratosphere-Troposphere Analyses of Regional Transport 2008 (START08) Experiment, *Bull. Amer. Meteor. Soc.*, 91, 327-342, doi: 10.1175/2009BAMS2865.1.

Pan, L.L., C.R. Homeyer, S.B. Honomichl, B.A. Ridley, M. Weisman, M. Barth, J.W. Hair, M.A. Fenn, C.F. Butler, G.S. Diskin, J.H. Crawford, T.B. Ryerson, I.B. Pollack, and H. Huntrieser, 2014. Thunderstorms Enhance Tropospheric Ozone by Wrapping and Shedding Stratospheric Air, *Geophys. Res. Lett.*, 41, 7785–7790, doi:10.1002/2014GL061921.

Pickering, K., et al., 2013. DISCOVER-AQ Houston 2013 mission web site (http://www-air.larc.nasa.gov/missions/discover-aq/discover-aq.html)

Siu, L.W., K.P. Bowman, C.C. Epifanio, 2015. Convective transport of trace species observed during the stratosphere-troposphere analyses of regional transport 2008 experiment (START08), *J. Geophys. Res.*, submitted.

Skamarock, W.C., J.B. Klemp, J. Dudhia, D.O. Gill, D.M. Barker, M.G. Duda, X.-Y. Huang, W. Wang, J.G. Powers, 2008. A Description of the Advanced Research WRF Version 3. Prepared by the National Center for Atmospheric Research, NCAR Technical Note NCAR/TN–475+STR (June).

Zhao, C., Y. Wang, T. Zheng, 2009. Summertime impact of convective transport and lightning NOx production over North America: modeling dependence on meteorological simulations. *Atmos. Chem. Phys.*, 9, 4315-4327, www.atmos-chem-phys.net/9/4315/2009/.